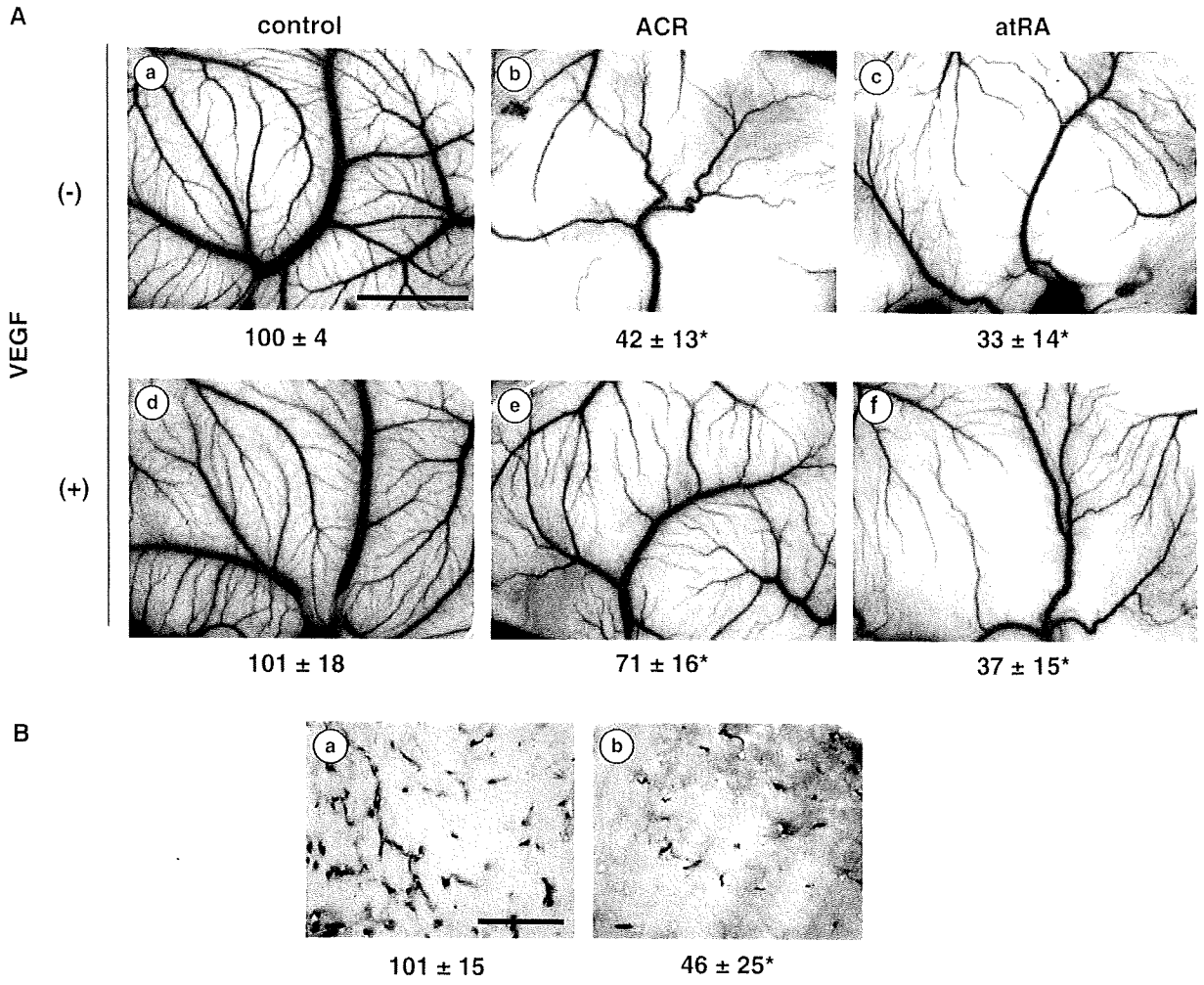

Figure 3 The antiangiogenic effect of ACR, but not of atRA, was rescued by simultaneous treatment with VEGF in CAM (**A**). The 4.5-day-old CAMs were treated with ACR and atRA for 48 h and then patterns of angiogenesis were photographed. Panel (**a**), vehicle (1% ethanol plus 1% DMSO); panel (**b**), 3 μg/egg ACR; panel (**c**), 500 ng/egg atRA; panel (**d**), vehicle plus 1 ng/egg mouse recombinant VEGF; panel (**e**), 3 μg/egg ACR plus 1 ng/egg mouse recombinant VEGF; panel (**f**) 500 ng/egg atRA plus 1 ng/egg mouse recombinant VEGF. Scale bar, 5 mm. Total numbers of branches of blood vessels were analyzed with angiogenesis-measuring software and are shown under each panel. A total of 18 eggs (6 eggs per experiment × 3 experiments) were evaluated and representative results are shown. (**B**) Matrigel plug assay: matrigel plugs containing 50 ng/ml VEGF ± 5 μM ACR were implanted into mice subcutaneously. One week later, matrigel plugs were collected and stained with hematoxylin and eosin (panels a and b). Panel **a**, VEGF alone (control); panel **b**, VEGF plus ACR. Representative data from a total of nine micrographs (3 fields × 3 mice) are presented. Scale bar, 500 μm. The number of invading cells in each micrograph was counted and the relative values are presented as percentages under each photograph. An asterisk indicates a significant difference ($P<0.05$) from the control. Panels **A** and **B** show representative results from two independent experiments, both of which gave similar results.

phosphorylation of VEGFR2 but rather increased it (compare lanes 4 with 6). Both ACR and atRA decreased the expression of VEGFR2 to about 70 and 60%, respectively, without VEGF treatment (compare lanes 1 with 2 and 3). However, this effect was not obvious in cells treated with VEGF (compare lanes 4–6). ACR did not affect the binding of VEGF to VEGFR2, nor did it affect *VEGF* mRNA levels (data not shown). On the other hand, pretreatment with ACR or atRA did not block the phosphorylation of FGFR1 but rather enhanced it (Figure 5b). Whereas ACR inhibited the phosphorylation of Ras, it did not inhibit the phosphorylation of Akt (Supplementary Figure 2). In addition, pretreatment with 5 μM ACR, but not with atRA, significantly inhibited the phosphorylation of ERK, which is induced downstream of VEGF stimuli (Figure 6a, lanes 5 and 6 in upper panel, respectively). The inhibition by ACR was inverted by the overexpression of constitutively active MAPK kinase in HUVECs (Figure 6b, lane 4 in upper panel).

Effect of ACR and atRA on HCC-Induced Angiogenesis in a Xenografted CAM Model

To confirm whether ACR and atRA have anti-HCC-induced angiogenic activity *in vivo*, we investigated the effect of ACR and atRA on HCC-induced angiogenesis in a xenografted

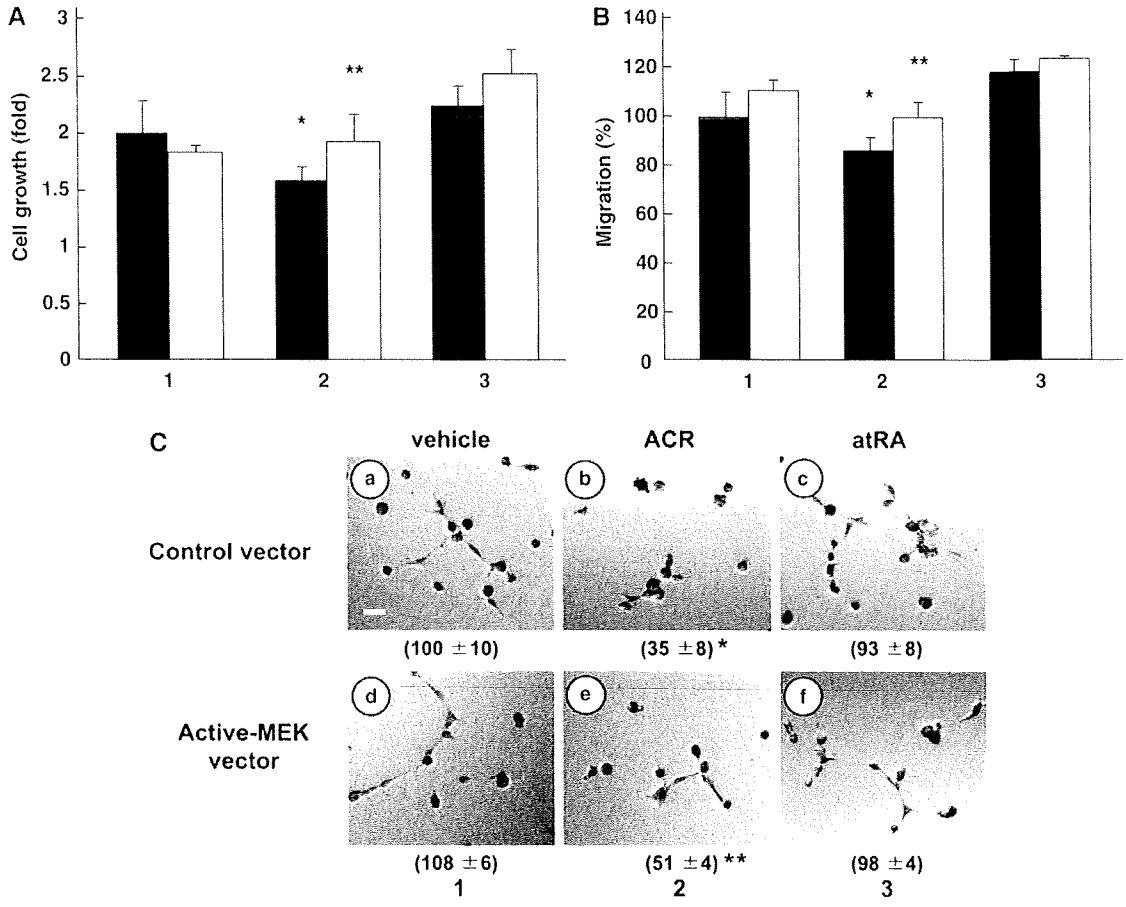

Figure 4 Effects of ACR and atRA on endothelial cell growth, migration, and tube formation. **(A)** HUVECs were transfected with a constitutively active MAPK kinase-expressing vector. After 2 days, cells (1×10^5 cells) were seeded onto 3.5-cm dishes and incubated for another 2 days. They were then incubated for 48 h in α-MEM medium containing 10% fetal calf serum, 100 ng/ml VEGF, and 5 μM ACR or atRA. Cells were counted and cell numbers are plotted as ploidy relative to values for untreated control cells at the start of incubation with ACR or atRA. Values represent means ± s.e. ($n = 2$). Lane 1, vehicle (0.1% ethanol); lane 2, ACR; lane 3, atRA. Closed columns, cells overexpressing control vector; open columns, cells overexpressing constitutively active MAPK kinase. A single asterisk indicates a significant difference ($P < 0.05$) from the control (lane 1, closed column) and double asterisks indicate a significant difference ($P < 0.05$) between samples with or without the overexpression of constitutively active MAPK kinase. **(B)** HUVECs were transfected with a constitutively active MAPK kinase-expressing vector. After 2 days, cells were wounded with a tip of pipette and incubated for 12 h in α-MEM medium containing 2.5% fetal calf serum, 100 ng/ml VEGF, and 5 μM ACR or atRA. The numbers of cells that migrated into the denuded area were counted and are plotted as percentages relative to values for untreated control cells. Values represent means ± s.e. ($n = 2$). Lane 1, vehicle (0.1% ethanol); lane 2, ACR; lane 3, atRA. Closed columns, cells overexpressing control vector; open columns, cells overexpressing constitutively active MAPK kinase. A single asterisk indicates a significant difference ($P < 0.05$) from the control (lane 1, closed column) and double asterisks indicate a significant difference ($P < 0.05$) between samples without or with the overexpression of constitutively active MAPK kinase. **(C)** HUVECs were transfected with a constitutively active MAPK kinase-expressing vector. After 2 days, cells were seeded onto polymerized matrigel at 2×10^5 cells/well. Thereafter, 100 ng/ml VEGF and 5 μM ACR or atRA were added, and incubated for 6 h. Patterns of tube formation were photographed. Scale bar, 100 μm. Panels (**a–c**), cells overexpressing control vector; panels (**d–f**), cells overexpressing constitutively active MAPK kinase. Panels (**a** and **d**), vehicle (0.1% ethanol) plus 100 ng/ml VEGF; panels (**b** and **e**), 5 μM ACR plus 100 ng/ml VEGF; panels (**c** and **f**), 5 μM atRA plus 100 ng/ml VEGF. The numbers of branches in each micrograph were counted and the relative values are presented as percentages under each photograph. A single asterisk indicates a significant difference ($P < 0.05$) from the control (panel **a** *vs* panel **b**) and double asterisks indicate a significant difference ($P < 0.05$) between samples with or without the overexpression of constitutively active MAPK kinase (panel **b** *vs* panel **e**). Panels **A–C** show representative results from two independent experiments, both of which gave similar results.

CAM model (Figure 7). Although 5 μM ACR inhibited HCC-induced angiogenesis by 37% (panel b), the same concentration of atRA did not show any inhibition at all (panel c). This result suggested that ACR, but not atRA, may prevent the recurrence of HCC in part through the inhibition of cancer angiogenesis.

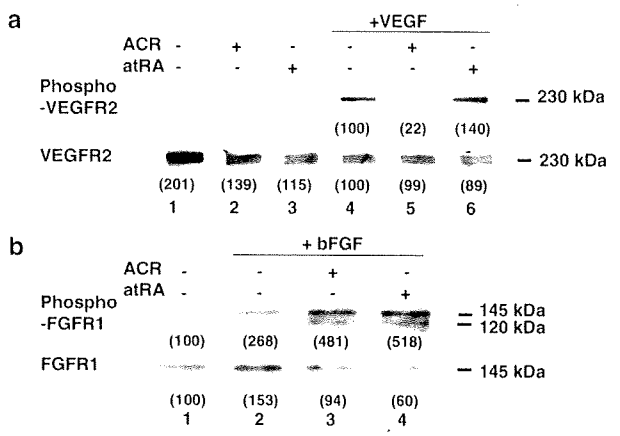

Figure 5 Effects of ACR and atRA on phosphorylation of growth factor receptors. After HUVECs had been incubated for 24 h with or without 5 μM ACR or atRA in medium containing 2.5% serum, cells were stimulated with either 100 ng/ml VEGF (panel **a**) or 50 ng/ml bFGF (panel **b**) for 5 min, and then lysed immediately. The amounts of each phosphorylated receptor (each upper bands), as well as whole amounts of each receptor (each lower bands), were assessed as described in the Materials and methods section. Panels **a** and **b** show representative results from two independent experiments, both of which gave similar results.

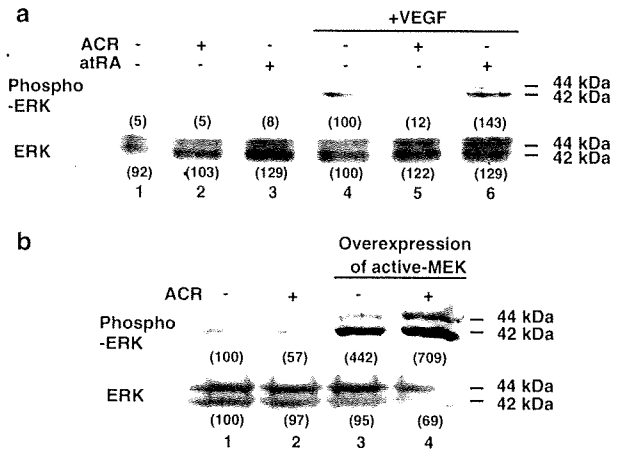

Figure 6 Effect of ACR on phosphorylation of ERK. (**a**) After HUVECs had been incubated for 24 h with or without 5 μM ACR or atRA in medium containing 2.5% serum, cells were stimulated with 100 ng/ml VEGF for 5 min and then lysed immediately. (**b**) HUVECs were transfected with a constitutively active *MEK* gene. The day after transfection, the medium was changed and cells were treated with 5 μM ACR and lysed immediately. The amounts of each phosphorylated ERK (upper bands), as well as whole amounts of ERK (lower bands), were assessed as described in the Materials and methods section.

DISCUSSION

In this paper, we have shown an antiangiogenic activity of ACR and its underlying molecular mechanism, differing from that of atRA. Although the relative antiangiogenic activity of ACR was about 10 times weaker than that of atRA at the same concentrations (Figure 1), ACR showed much stronger inhibition in endothelial cell growth, migration, and tube formation than atRA (Figure 4) because of suppression in the VEGF-MAPK pathway (Figures 5 and 6). ACR suppressed the phosphorylation of VEGFR2 (Figure 5a, lane 5). On the other hand, atRA induced the phosphorylation of VEGFR2 (Figure 5a, lane 6). This might be because of the induction of VEGF by atRA as reported previously.[17] ACR did not affect the levels of *VEGF* mRNA and the transactivation of the *VEGF* promoter (data not shown). ACR slightly inhibited the phosphorylation of VEGFR1 at 300 μM but not at all at 30 μM (Ishibashi *et al*, unpublished data). ACR (1 or 10 μM) did not inhibit other tyrosine kinases (for example, EGFR, FGFR3, FLT3, IGF1R, MET, PDGFR-α, PDGFR-β, and TRKB) (Ishibashi *et al*, unpublished data). Moreover, ACR inhibited the phosphorylation of Ras but not the phosphorylation of Akt (Supplementary Figure 2). Therefore, we speculate that ACR may selectively interfere with the phosphorylation of VEGFR2 after Ras activation, although it is not clear how ACR does this; the underlying detailed molecular mechanism(s) remain to be elucidated. ACR and atRA enhanced the phosphorylation of FGFR1 (Figure 5b, lanes 3 and 4). This result might be because of the induction of bFGF by atRA as previously reported.[18] ACR might also induce bFGF, probably through its retinoid activity.

These results suggest that suppression of the recurrence of HCC by ACR was induced in part through its antiangiogenic property by directly suppressing endothelial growth, migration, and tube formation through inhibition of the VEGFR2-MAPK axis. On the other hand, atRA inhibits angiogenesis by a disruption of vascular networks through an increased expression of Ang2 and inhibition in the Ang/Tie2 pathway.[6] Compared with atRA, ACR has 1/10–1/100 weaker 'retinoid' activities.[19] It has a 1/10 weaker action on leukemia differentiation,[20] and a 1/100 weaker carcinogenic action in transgenic mice that express the dominant-negative form of retinoic acid receptor.[21,22] On the other hand, accumulating evidence shows that ACR, but not atRA, has apoptosis-inducing activity in HCC cells, as well as in smooth muscle cells and vascular neointima.[23,24] We found that ACR acts as either a kinase inhibitor or a phosphatase stimulator and prevents hyperphosphorylation of RXR,[9] and now VEGFR2. In this context, we speculate that ACR resembles geranylgeraniol in terms of its isoprenoid-like structure, which has been implicated in the modulation of many phosphorylation/dephosphorylation signaling.[25,26]

Hepatocellular carcinoma is a major cause of cancer mortality worldwide, especially in Southeast Asia and in sub-Saharan Africa.[27] The development of HCC is frequently associated with a chronic inflammation of the liver induced by persistent infection with hepatitis B virus or hepatitis C virus. The annual incidence rises to ~20–25% in cirrhotic patients who have undergone a potentially curative removal of primary HCC in Japan; the recurrence rate at 5 years after the curative treatment may exceed 70%. This high recurrence rate is not because of local recurrence or metastasis from the original lesion, but rather from a second primary lesion.[19]

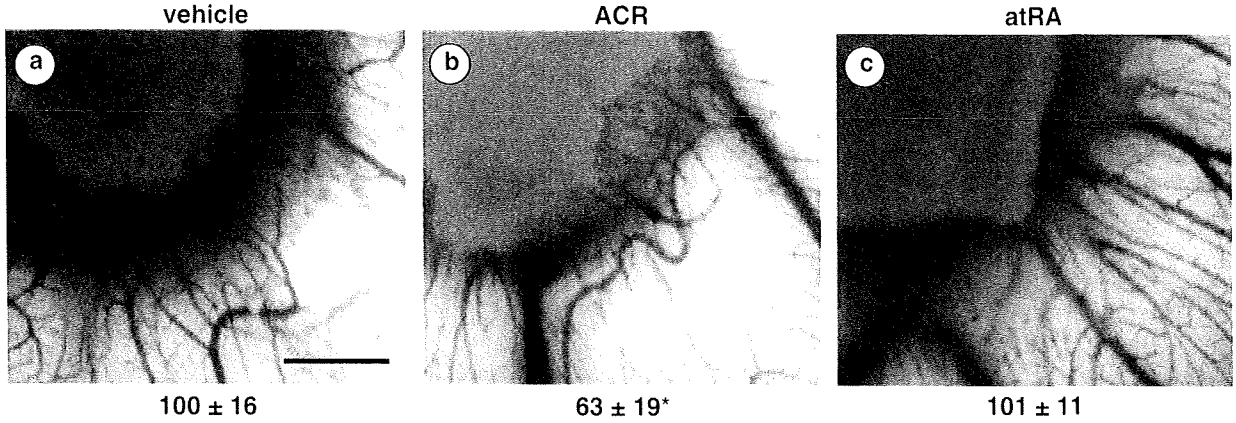

Figure 7 Effect of ACR on HCC-induced angiogenesis on CAM. HepG2 cell suspensions with or without 5 μM ACR or atRA were delivered at 4×10^5 cells per embryo onto the top of CAM on day 8 using a gelatin sponge implant. After a further 4-day incubation, a fat emulsion was injected into the chorioallantois, so that the vascular networks stood out against the white background of the lipid, and patterns of angiogenesis toward the implant were photographed. Panel (**a**), vehicle (1% EtOH); panel (**b**), 5 μM ACR; panel (**c**), 5 μM atRA. Scale bar, 1 mm. Total numbers of branches of blood vessels were counted and the relative values are presented as percentages under each photograph. An asterisk indicates a significant difference ($P<0.05$) from the control. This result shows the representative result from two independent experiments, both of which gave similar results.

In HCC tissues, RXR-α is constitutively phosphorylated by the activation of MAPK, resulting in a loss of its function and accumulation of inactive RXR-αs inside cells as dominant-negative inhibitors.[9,10] Therefore, phosphorylation of RXR-α causes a reduction in transactivation through a RAR/RXR complex.[9,28] ACR inhibits the phosphorylation of RXR-α and restores the function of RXR-α, and thereby transactivation through the RAR/RXR complex with endogenous retinoic acid. Retinoids are thought to activate the transcription of cell cycle inhibitor $p21^{CIP1}$ by RAR[29] and by apoptosis-inducer tissue transglutaminase in HCC.[19] However, 5 μM ACR hardly induces endothelial cell death (Figure 4A) and expression of $p21^{CIP1}$ mRNA levels in endothelial cells (data not shown). We found that phosphorylation of RAR/RXR was associated with the growth of endothelial cells and that ACR inhibited this phosphorylation (Supplementary Figure 3). As this phosphorylation of RAR/RXR coincided with the activation of VEGFR2 and Ras and as we had already found that RAR/RXR phosphorylation was induced by the overexpression of active MEK in cancer cells,[10] we speculate that phosphorylation of RAR/RXR would occur downstream of the VEGF/VEGFR axis in growing endothelial cells.

Acyclic retinoid suppressed both angiogenesis and HCC-induced angiogenesis in a xenografted CAM model (Figure 1, panels b–d and Figure 7, panel b, respectively). In this model, ACR did not affect the preexisting blood vessels on CAM. These results suggest that ACR did not affect the mature blood vessel and only affected neovasculature formation, including both normal angiogenesis and tumor angiogenesis. On the other hand, atRA suppressed angiogenesis but failed to suppress the tumor angiogenesis on CAM (Figures 1 and 7, panels e–g and panel c, respectively), suggesting that atRA inhibits angiogenesis in the embryonic stage, but not tumor-induced angiogenesis, and addressing the superiority of ACR as a promising antitumor angiogenesis agent. The dose of ACR used in this experiment (5 μM) is higher than the maximal blood concentration of ACR in clinical use (1 μM) (Ishibashi *et al*, unpublished data). However, we believe that liver tissue has higher doses of ACR than does the blood level because of the accumulation of ACR in the liver. These results suggest that one of the mechanisms of ACR action to prevent recurrence of HCC is its antiangiogenic activity.

Supplementary Information accompanies the paper on the Laboratory Investigation website (http://www.laboratoryinvestigation.org)

ACKNOWLEDGEMENTS

The authors thank Dr NG Ahn (University of Colorado, CO) for providing the constitutively active MAPK kinase vector. This study was supported in part by grants from the Chemical Genomics Research Project from RIKEN (to SK) and Grant-in-Aids from the Ministry of Education, Science, Sports, and Culture (17015016, HM).

DISCLOSURE/CONFLICT OF INTEREST

The authors declare no conflict of interest.

1. Mazitschek R, Giannis A. Inhibitors of angiogenesis and cancer-related receptor tyrosine kinase. Curr Opin Chem Biol 2004;8:432–441.
2. Ferrara N, Kerbel R. Angiogenesis as a therapeutic target. Nature 2005;438:967–974.
3. Chambon P. A decade of molecular biology of retinoic acid receptors. FASEB J 1996;10:940–954.
4. Obora A, Shiratori Y, Okuno M, *et al.* Synergistic induction of apoptosis by acyclic retinoid and interferon-β in human hepatocellular carcinoma cells. Hepatology 2002;36:1115–1124.
5. Altucci L, Leibowitz MD, Ogilvie KM, *et al.* RAR and RXR modulation in cancer and metabolic disease. Nat Rev Drug Discov 2007;6:793–810.
6. Suzuki Y, Komi Y, Ashino H, *et al.* Retinoic acid controls blood vessel formation by modulating endothelial and mural cell interaction via suppression of Tie2 signaling in vascular progenitor cells. Blood 2004;104:166–169.

7. Altucci L, Gronemever H. The promise of retinoids to fight against cancer. Nat Rev Cancer 2001;1:181–193.
8. Muto Y, Moriwaki H, Ninomiya M, *et al.* Prevention of second primary tumors by an acyclic retinoid, polyprenoic acid, in patients with hepatocellular carcinoma. N Engl J Med 1996;334: 1561–1568.
9. Matsushima-Nishiwaki R, Okuno M, Takano Y, *et al.* Molecular mechanism for growth suppression of human hepatocellular carcinoma cells by acyclic retinoid. Carcinogenesis 2003;24: 1353–1359.
10. Matsushima-Nishiwaki R, Okuno M, Adachi S, *et al.* Phosphorylation of retinoid X receptor α at serine 260 impairs its metabolism and function in human hepatocellular carcinoma. Cancer Res 2001;61: 7675–7682.
11. Kagawa M, Tetsuo S, Ishibashi N, *et al.* An acyclic retinoid, NIK-333, inhibits *N*-diethylnitrosamine-induced rat hepatocarcinogenesis through suppression of TGF-α expression and cell proliferation. Carcinogenesis 2004;25:979–985.
12. Komi Y, Suzuki Y, Shimamura M, *et al.* Mechanism of inhibition of tumor angiogenesis by β-hydroxyisovalerylshikonin. Cancer Sci 2009;100:269–277.
13. Mansour SJ, Matten WT, Hermann AS, *et al.* Transformation of mammalian cells by constitutively active MAP kinase kinase. Science 1994;265:966–970.
14. Komi Y, Ohno O, Suzuki Y, *et al.* Inhibition of tumor angiogenesis by targeting endothelial surface ATP synthase with sangivamycin. Jpn J Clin Oncol 2007;37:867–873.
15. Rabatti D, Nico B, Vacca A, Presta M. The gelatin sponge-chorioallantoic membrane assay. Nat Protoc 2006;1:85–91.
16. Chen MJ, Chiou PP, Lin P, *et al.* Suppression of growth and cancer-induced angiogenesis of aggressive human breast cancer cells (MDA-MB-231) on the chorioallantoic membrane of developing chicken embryos by E-peptide of pro-IGF-I. J Cell Biochem 2007;101:1316–1327.
17. Saito A, Sugawara A, Uruno A, *et al.* All-trans retinoic acid induces *in vitro* angiogenesis via retinoic acid receptor: possible involvement of paracrine effects of endogenous vascular endothelial growth factor signaling. Endocrinology 2007;148:1412–1423.
18. Gaetano C, Catalano A, Illi B, *et al.* Retinoids induce fibroblast growth factor-2 production in endothelial cells via retinoic acid receptor α activation and stimulate angiogenesis *in vitro* and *in vivo*. Circ Res 2001;88:E38–E47.
19. Kojima S, Okuno M, Matsushima-Nishiwaki R, *et al.* Acyclic retinoid in the chemoprevention of hepatocellular carcinoma (Review). Int J Oncol 2004;24:797–805.
20. Tsurumi H, Tojo A, Takahashi T, *et al.* Differentiation induction of human promyelocytic leukemia cells by acyclic retinoid (polyprenoic acid). Int J Hematol 1993;59:9–15.
21. Sakabe T, Tsuchiya H, Endo M, *et al.* An antioxidant effect by acyclic retinoid suppresses liver tumor in mice. Biochem Pharmacol 2007;73:1405–1411.
22. Yanagitani A, Yamada S, Yasui S, *et al.* Retinoic acid receptor α dominant negative form causes steatohepatitis and liver tumors in transgenic mice. Hepatology 2004;40:366–375.
23. Nakamura N, Shidoji Y, Yamada Y, *et al.* Induction of apoptosis by acyclic retinoid in the human hepatoma-derived cell line, HuH-7. Biochem Biophys Res Commun 1995;207:382–388.
24. Kada N, Suzuki T, Aizawa K, *et al.* Acyclic retinoid inhibits neointima formation through retinoic acid receptor beta-induced apoptosis. Arterioscler Thromb Vasc Biol 2007;27:1535–1541.
25. Nakajo S, Okamoto M, Masuda Y, *et al.* Geranylgeraniol causes a decrease in levels of calreticulin and tyrosine phosphorylation of a 36-kDa protein prior to the appearance of apoptotic features in HL-60 cells. Biochem Biophys Res Commun 1996;226:741–745.
26. Hashimoto K, Morishige K, Sawada K, *et al.* Geranylgeranylacetone inhibits lysophosphatidic acid-induced invasion of human ovarian carcinoma cells *in vitro*. Cancer 2005;103:1529–1536.
27. Ince N, Wands JR. The increasing incidence of hepatocellular carcinoma. N Engl J Med 1999;340:798–799.
28. Solomon C, White JH, Kremer R. Mitogen-activated protein kinase inhibits 1,25-dihydroxyvitamin D3-dependent signal transduction by phosphorylating human retinoid X receptor α. J Clin Invest 1999;103:1729–1735.
29. Liu M, Iavarone A, Freedman LP. Transcriptional activation of the human p21(WAF1/CIP1) gene by retinoic acid receptor. J Biol Chem 1996;271:31723–31728.

Cancer Research

PSF1, a DNA Replication Factor Expressed Widely in Stem and Progenitor Cells, Drives Tumorigenic and Metastatic Properties

Yumi Nagahama[1], Masaya Ueno[1], Satoru Miyamoto[1], Eiichi Morii[2], Takashi Minami[4], Naoki Mochizuki[3], Hideyuki Saya[5], and Nobuyuki Takakura[1]

Abstract

PSF1 (partner of sld five 1) is an evolutionarily conserved DNA replication factor implicated in DNA replication in lower species that is strongly expressed in a wide range of normal stem cell populations and progenitor cell populations. Because stem and progenitor cells possess high proliferative capacity, we hypothesized that PSF1 may play an important role in tumor growth. To begin to investigate PSF1 function in cancer cells, we cloned the mouse PSF1 promoter and generated lung and colon carcinoma cells that stably express a PSF1 promoter-reporter gene. Reporter expression in cells correlated with endogenous PSF1 mRNA expression. In a tumor cell xenograft model, high levels of reporter expression correlated with high proliferative activity, serial transplantation potential, and metastatic capability. Notably, cancer cells expressing reporter levels localized to perivascular regions in tumors and displayed expression signatures related to embryonic stem cells. RNAi-mediated silencing of endogenous PSF1 inhibited cancer cell growth by disrupting DNA synthesis and chromosomal segregation. These findings implicate PSF1 in tumorigenesis and offer initial evidence of its potential as a theranostic target. *Cancer Res; 70(3); 1215–24. ©2010 AACR.*

Introduction

PSF1 (partner of SLD5) is a member of the tetrameric complex termed GINS, composed of SLD5, PSF1, PSF2, and PSF3, and is well conserved evolutionarily. In yeast, the GINS complex associates with the MCM2-7 complex and CDC45, and this "C-M-G complex" (CDC45-MCM2-7-GINS) regulates both the initiation and the progression of DNA replication (1–6). In *Xenopus* and human, GINS has been suggested to be involved in DNA replication because of its binding to DNA replication protein (7–10); however, a recent study suggests that PSF1/2 is associated with the response to replication stress and acquisition of DNA damage in untransformed human dermal fibroblasts (11). Thus, the exact functions of GINS components in mammalian cells are not yet clear.

Authors' Affiliations: [1]Department of Signal Transduction, Research Institute for Microbial Diseases, Osaka University; [2]Department of Pathology, Osaka University School of Medicine; [3]Department of Structural Analysis, National Cardiovascular Center Research Institute, Suita, Osaka, Japan; [4]Laboratory for Systems Biology and Medicine, Research Center for Advanced Science and Technology (LSBM), University of Tokyo, Meguro, Tokyo, Japan; and [5]Division of Gene Regulation, Institute for Advanced Medical Research, Keio University School of Medicine, Shinjyuku-ku, Tokyo, Japan

Note: Supplementary data for this article are available at Cancer Research Online (http://cancerres.aacrjournals.org/).

Corresponding Author: Nobuyuki Takakura, Department of Signal Transduction, Research Institute for Microbial Diseases, Osaka University, 3-1 Yamada-oka, Suita, Osaka 565-0871, Japan. Phone: 81-6-6879-8312; Fax: 81-6-6879-8314; E-mail: ntakaku@biken.osaka-u.ac.jp.

doi: 10.1158/0008-5472.CAN-09-3662

We have previously cloned the mouse ortholog of *PSF1* from a hematopoietic stem cell cDNA library (12) and found that PSF1 expression in mice was predominantly observed in the adult bone marrow and thymus, as well as the testis and ovary (i.e., tissues in which stem cell proliferation is actively induced and continues after birth). Moreover, we reported that PSF1 is strongly expressed in different immature cell lineages, such as cells in the inner cell mass during early embryogenesis as well as spermatogonia and hematopoietic stem cells after birth (12–14). Loss of PSF1 led to embryonic lethality around the implantation stage caused by the inability of cells of the inner cell mass to proliferate (12). Moreover, haploinsufficiency of PSF1 in $PSF1^{+/-}$ mice resulted in the delayed induction of hematopoietic stem cell proliferation during reconstitution of bone marrow after 5-fluorouracil ablation. These data strongly suggest that PSF1 is required for acute proliferation of cells, especially immature cells such as stem cells and progenitor cells.

Several recent studies have suggested that GINS components play a role not only in immature cells from normal tissues, as we reported, but also in cancer cells. For example, all GINS components were found to be overexpressed in intrahepatic cholangiocarcinoma tissues (15). A Gene Expression Omnibus (GEO) database search revealed that *PSF1* is an estrogen target in MCF7 human breast carcinoma cells (16). In a comprehensive study, it was found that *PSF1* and *SLD5* were upregulated in aggressive melanoma (17). Based on these results, we examined the nature of cells highly expressing PSF1 in a tumor xenograft model.

Genetic events caused by epigenetic modulation and microenvironmental exposure have been suggested to be responsible

for tumor progression. Therefore, a species-matched (murine) microenvironment is needed to examine the nature of cells strongly expressing PSF1.

Here, we have investigated the expression of PSF1 and the localization of PSF1-positive cancer cells in a mouse tumor cell xenograft model. We observed malignant behavior of highly PSF1-positive tumor cells with regard to tumorigenesis and metastasis. Moreover, highly PSF1-positive cancer cells have been characterized by microarray analysis, and the data compared with those of the recently reported embryonic stem cell (ESC)–like gene expression signature in poorly differentiated aggressive human tumors (18). Finally, to determine whether PSF1 could be a molecular target for the development of anticancer drugs, we silenced the *PSF1* gene by the RNA interference (RNAi) method in human carcinoma cell lines and observed the effects thereof on the growth of the cancer cells.

Materials and Methods

Cell culture and cell line construction. LLC, B16, NIH3T3, HeLa, and HEK293T were maintained in DMEM (Sigma) with 10% fetal bovine serum (FBS; Sigma) and penicillin/streptomycin (Life Technologies, Inc.). Colon26 cells were maintained in RPMI 1640 (Sigma) with 10% FBS and penicillin/streptomycin. Mouse embryonic fibroblasts were prepared from day 14.5 embryos and cultured in high-glucose DMEM (Sigma) with 10% FBS and penicillin/streptomycin.

The gene encoding the PSF1 promoter region was isolated by mouse BAC cloning (RP23-193L22, Advanced GenoTechs Co.). Using the 5′ upstream sequence of the first exon of the *PSF1* locus as a probe, 5.5 kb of the 5′flanking PSF1 gene were isolated and subcloned into pBluescript II KS (Stratagene). The enhanced green fluorescent protein (*EGFP*) gene and the *neomycin* gene were excised from pEGFP-N1 and pcDNA3.1(−) (Clontech), respectively, and ligated to the 5.5 kb of the PSF1 5′-flanking fragment. This construct was designated *PSF1p-EGFP*. LLC and colon26 cells were transfected using Lipofectamine 2000 (Invitrogen). After transfection, the cells were cultured in medium supplemented with G418 (Life Technologies) to obtain cells stably expressing EGFP under the control of the PSF1 promoter (LLC-*PSF1p-EGFP* and colon26-*PSF1p-EGFP*).

Quantitative reverse transcription-PCR. Quantitative reverse transcription-PCR (RT-PCR) was done as previously described (14). The primer sets were described in Supplementary Materials and Methods.

Mice. Seven- to eight-week-old C57BL/6 female mice (for the LLC experiments) and BALB/c female mice of the same age (for colon26) were purchased from Japan SLC. All animal studies were approved by the Osaka University Animal Care and Use Committee. Subcutaneous xenografts were established by injecting 10^6 cells into the flanks of the mice.

Flow cytometric analysis. Single-cell suspensions from tumors were prepared using a standard protocol. Cell sorting was done using a FACSAria (Becton Dickinson). For the EGFP^{high} population, the 5% most brightly fluorescing cells were sorted, and for the EGFP^{low} population, the 5% least fluorescent. We used parental LLC or colon26 as negative controls.

In vitro *clonal analyses and* in vivo *tumorigenicity analysis.* Isolated cells were plated on 10-cm culture dishes (200 per dish for LLC-*PSF1p-EGFP* and 100 per dish for colon26-*PSF1p-EGFP*) and cultured. The percentage of cells that initiated a clone was taken as the plating efficiency. For *in vivo* experiments, 100 sorted cells in 100 μL of PBS with growth factor–reduced Matrigel (BD Biosciences; 1:1) were injected s.c. into the mice. Five weeks after injection, tumor volumes were measured with a caliper and calculated as width × width × length × 0.52.

Invasion assay and metastasis assay. The invasive activity of tumor cells was assayed using a BioCoat Matrigel Invasion Chamber (BD Biosciences) according to the manufacturer's instruction.

For the lung metastasis assay using LLC-*PSF1p-EGFP*, 10^5 viable sorted cells were injected into the tail veins of mice. After 4 wk, lungs were dissected and the number of colonies observable on the surface of the lungs was noted. For the hepatic metastasis assay of colon26-*PSF1p-EGFP*, spleens of mice were exposed to allow the direct injection of 5×10^4 viable sorted cells. After 12 d, livers and spleens were dissected out and the number of colonies observable on the surface of the livers was recorded. Sections of liver were stained with H&E to evaluate tissue morphology and to detect metastases.

Immunohistochemistry and immunocytochemistry. Immunohistochemical analyses were done as previously described (19). Rabbit anti-GFP antibody (Invitrogen) and rat anti-CD31 (BD Biosciences) were used for primary antibodies. For the fluorescent immunohistochemical analyses, phycoerythrin-conjugated anti-CD31 (BD Biosciences) was used for staining endothelial cells.

For immunocytochemistry, anti-PSF1(14), anti-bromodeoxyuridine (BrdUrd) (Zymed Laboratories), anti–β-tubulin (Sigma), anti–CENP-A (MBL), and anti-survivin (Chemicon International, Inc.) antibodies were used as previously described (14).

PSF1 *knockdown.* Transfection was done using Lipofectamine 2000 (Invitrogen). For the enrichment of transiently shRNA vector–transfected cells, the puromycin resistance gene was ligated into the *Xho*I site of the pSINsi-hU6 vector (Takara), and then sense and antisense oligonucleotide pairs (see below) were annealed and ligated into the *Bam*HI/*Cla*I site of the pSINsi-hU6-P vectors. The sequences of the oligonucleotide sets were described in Supplementary Materials and Methods. For time-lapse imaging of histone H3 and tubulin in living cells, HEK293T cells were transfected with GFP-histone (20) or tubulin-GFP (Clontech) expression vectors, and stably expressing clones were selected. Time-lapse observation was done as previously reported using an IX70 microscope (Olympus; ref. 21).

Microarray and bioinformatics analysis. Microarrays were done as previously described (22). Raw data are available for download from GEO (GSE17112). Gene set enrichment analysis (GSEA; ref. 23) was done by CeresBioscience as previously reported.

Statistical analysis. Results were expressed as the mean ± SEM. Student's *t* test was used for statistical analysis. Differences were considered statistically significant when $P < 0.01$.

Results

Establishment of transgenic cell lines to monitor endogenous* PSF1 *expression in living cells. We first examined *PSF1* mRNA expression in mouse cancer cell lines, a noncancer cell line, and primary cultured cells. *PSF1* mRNA in cancer cell lines is expressed to a greater degree than in the noncancer cell line or primary cultured cells (Fig. 1A). To determine whether the cancer cells strongly expressing PSF1 had malignant features, they need to be collected as living cells. Because PSF1 is an intracellular protein, viable cells cannot be isolated using PSF1 antibody and flow cytometric cell sorting. Therefore, we used promoter activity to monitor the expression level of PSF1 in cancer cells in the murine tumor xenograft model. We have cloned the mouse *PSF1* promoter gene and established lung carcinoma [Lewis lung carcinoma (LLC)] and colon cancer (colon26) cell lines stably expressing EGFP under the transcriptional control of the *PSF1* promoter (LLC- and colon26-*PSF1p-EGFP*, respectively). We confirmed *PSF1* mRNA expression in parental LLC and colon26 cells (data not shown). After inoculation of LLC-*PSF1p*-EGFP, tumors were dissected and the intensity of EGFP in dissociated cancer cells was analyzed by flow cytometry (Fig. 1B–D). As can be seen, EGFP-positive ($EGFP^+$) cells containing high or low levels of EGFP ($EGFP^{high}$ or $EGFP^{low}$ cells, respectively) were present. These were separated and the expression of *PSF1* mRNA was examined (Fig. 1D). The results indicate that the intensity of EGFP is correlated with the endogenous *PSF1* expression. Similar results were obtained using colon26-*PSF1p-EGFP* (data not shown). These results suggest that these cell lines are useful tools to monitor endogenous *PSF1* expression in living cells.

EGFP(PSF1)^{high} cells possess greater tumorigenic capacity. To study their colony forming efficiency, cancer cells

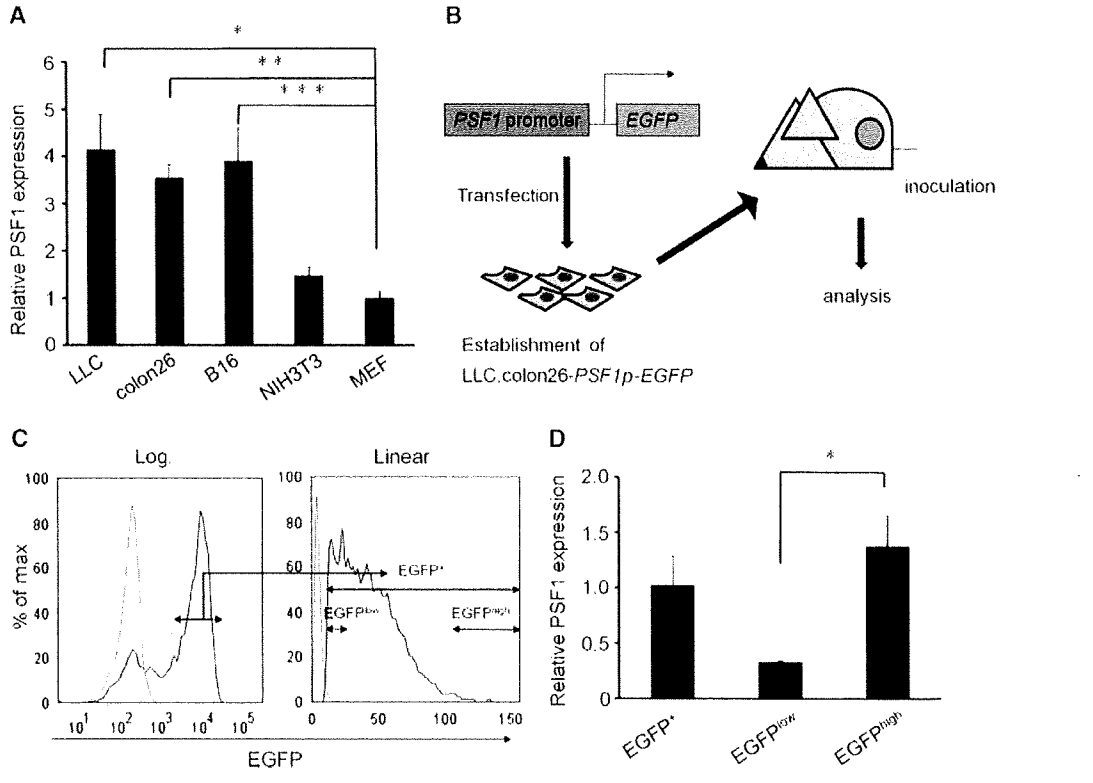

Figure 1. PSF1 expression in murine carcinoma cell lines. A, expression of *PSF1* mRNA in murine carcinoma cells. Total RNA was analyzed by quantitative RT-PCR for *PSF1* expression in different murine carcinoma cell lines and compared with a noncancer cell line and a primary cell culture. The values are normalized to the amount of mRNA in mouse embryonic fibroblasts. *LLC*, lung carcinoma; *colon26*, colon carcinoma; *B16*, melanoma; *NIH3T3*, mouse embryonic fibroblast cell line; *MEF*, mouse embryonic fibroblast. Data show the mean ± SEM. *, **, ***, $P < 0.01$ ($n = 3$). B, experimental procedure. We have cloned the mouse *PSF1* promoter gene and established cell lines stably expressing EGFP under the transcriptional control of the *PSF1* promoter (LLC- and colon26-*PSF1p-EGFP*, respectively). After inoculation of LLC- or colon26-*PSF1p*-EGFP, tumors were dissected and the dissociated cancer cells were separated using a cell sorter according to the intensity of EGFP expression and further analyzed. C, fluorescence-activated cell sorting analysis of cells from tumor tissues injected with LLC (green) or LLC-*PSF1p-EGFP* (red) cells. $EGFP^+$, $EGFP^{low}$, and $EGFP^{high}$ cells were sorted as indicated. Intensity of EGFP is displayed on a log or linear scale. D, quantitative RT-PCR analysis of *PSF1* mRNA expression in sorted cells as indicated. The values are normalized to the amount of mRNA in $EGFP^+$ cells. Data show the mean ± SEM. *, $P < 0.01$ ($n = 3$).

(LLC- and colon26-*PSF1p-EGFP*) from tumor-bearing mice were divided into three fractions (EGFP$^+$, EGFP^{low}, and EGFP^{high}) as indicated in Fig. 1C, seeded, and cultured for 2 weeks. EGFP^{high} cells formed significantly larger colonies than did EGFP^{low} cells (Fig. 2A) in both colon26 and LLC tumors.

We next examined the serial transplantation ability of these cells. We inoculated sorted EGFP^{high} or EGFP^{low} cells from tumor-bearing mice into new hosts to evaluate the relationship between PSF1 expression and tumorigenicity. Four weeks (LLC-*PSF1p-EGFP*) or 2 weeks (colon26-*PSF1p-EGFP*) after initial inoculation, 100 sorted EGFP$^+$, EGFP^{low}, or EGFP^{high} tumor cells were again transplanted into new hosts. EGFP^{high} cells from both LLC and colon26 tumors formed significantly larger tumors than did EGFP^{low} or EGFP$^+$ cells (Fig. 2B). When tumor cell components were examined in tumors generated after the second transplantation, EGFP^{high} cells were found to have given rise to both EGFP^{high} and EGFP^{low} cells in both LLC and colon26 tumors (Supplementary Fig. S1). Taken together, these data suggest that cancer cells expressing higher levels of *PSF1* exhibit high cloning efficiency and tumorigenicity.

EGFP(PSF1)^{high} cells possess greater invasive and metastatic capacity. We investigated that EGFP^{high} cells also play a crucial role in tumor metastasis. We determined the overall ability of cells sorted, as described in Fig. 1C, for invasion using Matrigel, a basement membrane model used to estimate metastatic potential. EGFP^{high} cells migrated more effectively than did EGFP^{low} cells or EGFP$^+$ cells, indicating that they possess greater invasive capacity (Fig. 3A and B).

Next, we examined the *in vivo* metastatic potential of these cells by two different means. First, viable sorted EGFP^{high} or EGFP^{low} cells from LLC tumors were injected into the tail veins of recipient mice. After 4 weeks, macrometastatic lesions

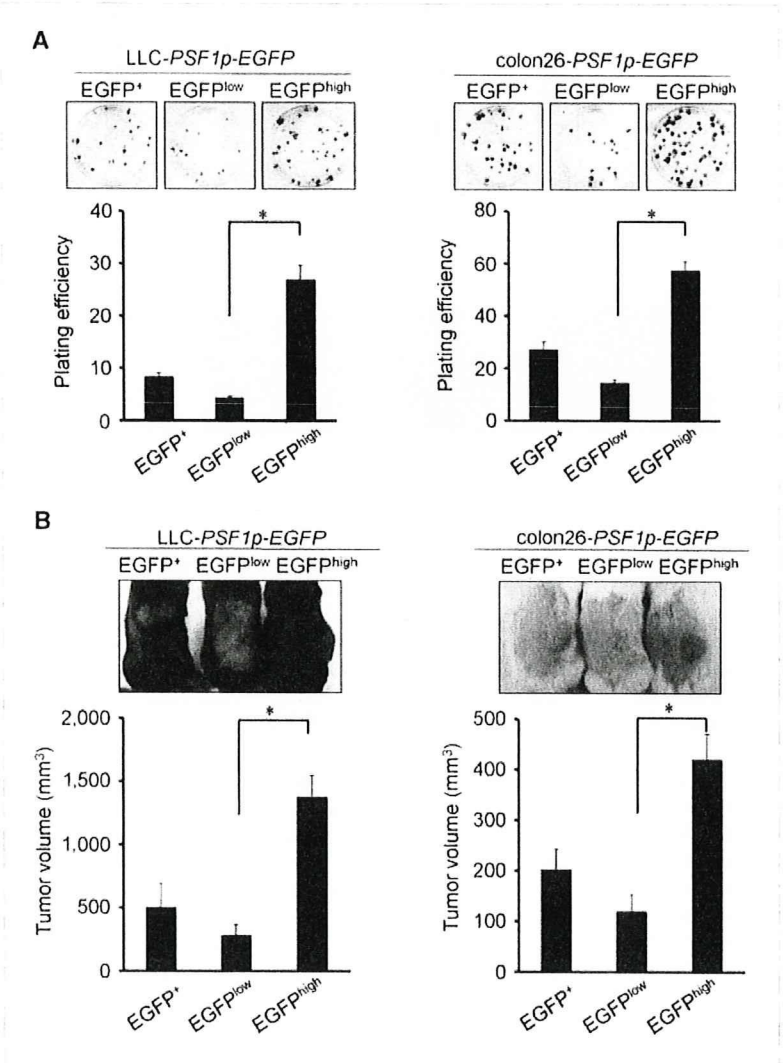

Figure 2. High proliferative ability of PSF1^{high} cancer cells. A, plating efficiency of sorted cells. Sorted cells from tumor tissues injected with LLC-*PSF1p-EGFP* or colon26-*PSF1p-EGFP* were seeded onto 10-cm culture dishes and cultured for 2 wks. Colonies generated from different fractions as indicated were stained with Giemsa solution (top). Quantitative evaluation of colonies from each fraction as indicated. Percentages of the colony numbers relative to the number of cells seeded are presented (bottom). Data show the mean ± SEM. *, $P < 0.01$ ($n = 3$). Results shown are representative of at least three independent experiments. B, tumorigenesis assay. Gross appearance of the tumor mass in mice 5 wks after inoculation with sorted cancer cells as indicated (top). Tumor volume was determined 5 wks after inoculation with sorted cells as indicated (bottom). Data show the mean ± SEM. *, $P < 0.01$ ($n = 10$). Experiments were done at least three times with similar results.

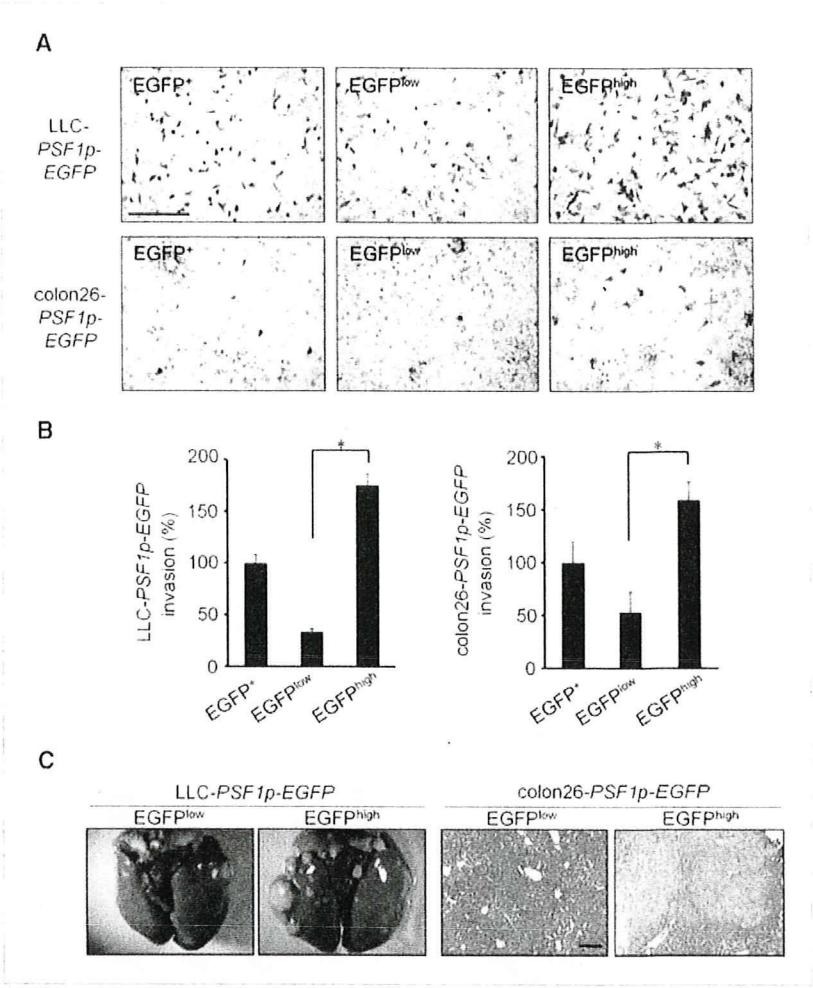

Figure 3. Invasive and metastatic capacity of LLC-*PSF1p-EGFP* and colon26-*PSF1p-EGFP*. A, representative images of sorted cells that migrated across a Matrigel-coated membrane. Bar, 200 μm. B, quantitative evaluation of the migrated cells: percentage of migrated cells relative to the applied total cell number normalized with the data from EGFP$^+$ cells. Data show the mean ± SEM. *, $P < 0.01$ ($n = 3$). Results shown are representative of at least three independent experiments. C, metastasis analysis. Gross appearance of lung metastases after injection with sorted EGFP^{low} or EGFP^{high} cells from LLC tumor (left). Liver metastases after injection with sorted EGFP^{low} or EGFP^{high} cells from colon26 tumor (right). Bar, 200 μm. Results shown are representative of at least three independent experiments.

in the lung were enumerated. Results clearly indicated that EGFP^{high} cells had a higher metastatic potential than did EGFP^{low} cells (Fig. 3C; Supplementary Fig. S2A). Second, in the case of colon26 tumors, viable sorted EGFP^{high} or EGFP^{low} cells were injected into the spleen. After 12 days, metastatic nodules in the liver were analyzed on liver sections. EGFP^{low} cells rarely generated metastatic foci, but large lesions were frequently observed in the livers of mice injected with EGFP^{high} cells (Fig. 3C; Supplementary Fig. S2B).

ESC-like signatures are enriched in EGFP^{high} cells versus EGFPlow cells. Recent studies showed that poor prognosis in a diverse set of human and mouse malignancies is associated with the expression of an ESC-like genetic program (18). We therefore compared the gene expression signatures of EGFP^{low} and EGFP^{high} cells. Data clearly indicated that ESC-like signatures were enriched in EGFP^{high} cells versus EGFP^{low} cells (Fig. 4). Interestingly, other ESC-like signatures (24, 25), in which some cancer-initiating/stem cells (CIC/CSC) were enriched, were also enriched in EGFP^{high} cells versus EGFP^{low} cells (Fig. 4; Supplementary Table S1). Taken together, the results from all the above experiments lead us to conclude that cancer cells harboring large amounts of PSF1 or high transcriptional activity of *PSF1* possess malignant features, including high proliferative capacity, tumorigenesis, metastatic ability, and genetic profiles of poor prognosis.

PSF1^{high} cells are localized in perivascular regions. Next, the tissue distribution of EGFP^{high} cells in tumors was examined (Fig. 5A–C). EGFP^{high} cells were located close to the edge of the tumor and near the blood vessels. Preliminary, we investigated PSF1 expression in human carcinoma specimens (Supplementary Fig. S3). We found that PSF1 expression in human lung and esophageal squamous cell carcinoma specimens was confined to the surrounding basal-like cells and located at some distance from the centers of terminal differentiation zones. Furthermore, PSF1-positive cells were located in close proximity to blood vessels near the edge of the tumor, as observed in our murine xenograft model (Supplementary Fig. S3).

Silencing of PSF1 inhibits the proliferation of carcinoma cells. Targeted disruption of PSF1 led to embryonic lethality

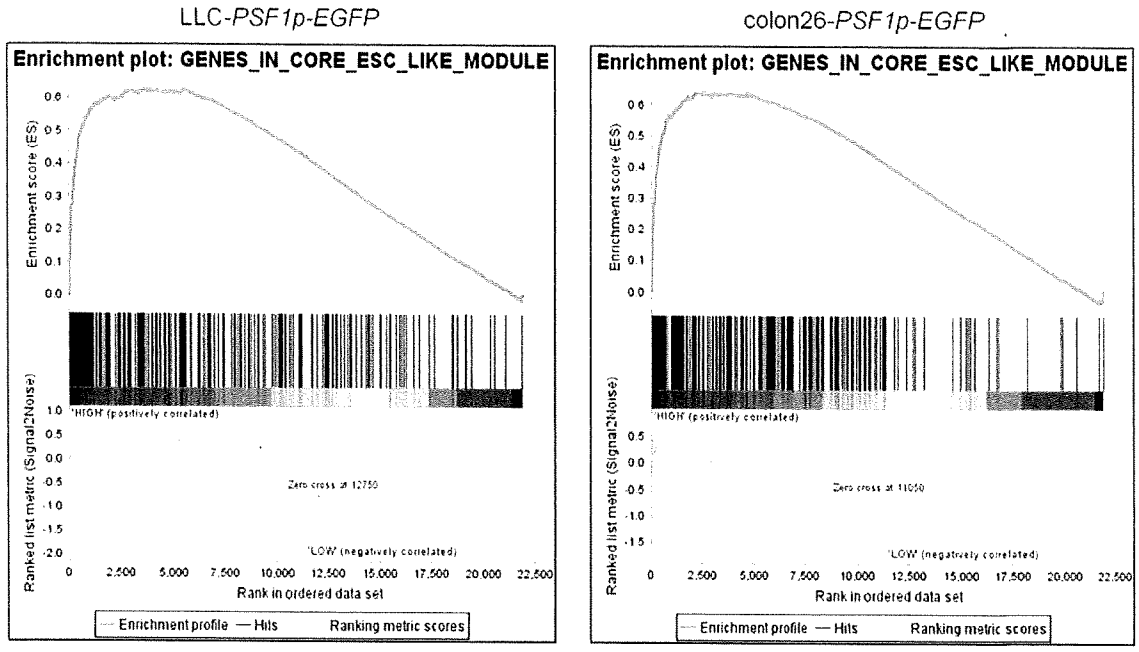

Figure 4. Gene set enrichment analysis. GSEA plots show that expression of an ESC-like core gene module (24) is more enriched in EGFP^{high} cells compared with EGFP^{low} cells in LLC-*PSF1p-EGFP* tumor and colon26-*PSF1p-EGFP* tumor.

caused by the inhibition of cell growth in the inner cell mass (12), suggesting that silencing this gene may also inhibit tumor cell proliferation. To determine whether PSF1 could be a suitable molecular target for anticancer drug development, the inhibitory effects of its expression in human carcinoma cell lines should be evaluated. In budding yeast, it has been suggested that PSF1 plays a role in DNA replication, associated with the formation of the DNA replication fork (7–9). However, its function in mammalian cells has not been clarified. First, we established the cellular localization of PSF1 in HeLa cells (Fig. 6A). At interphase, PSF1 was localized predominantly in the nuclei. During mitosis, it was almost exclusively diffusely located outside the chromatin. Next, we used short hairpin RNA (shRNA) expression plasmids for RNAi-mediated endogenous gene silencing in HeLa cells *in vitro*. Quantitative RT-PCR with gene-specific shRNA confirmed that endogenous PSF1 gene expression was reduced by more than 75% within 72 hours, compared with the lack of effect of transfection of a scrambled shRNA expression plasmid (data not shown). At 96 hours, the total number of PSF1 shRNA–treated cells was significantly decreased compared with the control (Fig. 6B), suggesting that depletion of PSF1 had resulted in cell growth arrest. To analyze more precisely the effect of PSF1 depletion on cell growth, first, the DNA contents were analyzed (Fig. 6C, left). Results showed that depletion of PSF1 led to an increase in the fraction of cells in the sub-G_1, S, and G_2-M phases, suggesting that this molecule is important not only for S phase but also for G_2-M phase progression.

Polyploid cells can arise as a result of errors in mitosis. These cells usually exit the cycle in an aberrant fashion, without sister chromatid segregation or cytokinesis, a process known as "mitotic slippage." Cancer cell lines (such as HeLa and HEK293T cells) lacking functional p53 progress into S phase without p53-dependent growth arrest at the subsequent G_1-S boundary, and hyperploid cells develop as a result. However, no obvious hyperploid cell populations were found in PSF1-depleted cells (Fig. 6C, left). During a 4-hour pulse, approximately 75% of scrambled shRNA–treated cells incorporated BrdUrd (Fig. 6C, right), but only approximately 23% of PSF1-depleted cells possessed large nuclei staining with anti-BrdUrd antibody. Taken together, these data indicate that PSF1 depletion also inhibits DNA synthesis of multiploid cells, which resulted in the generation of only a small number of cells harboring large nuclei (8N; Fig. 6C, left).

During the 72- to 120-hour period after shRNA treatment, the population of G_2-M phase cells increased in the PSF1 depletion experiments (Fig. 6C, left). Therefore, we assessed the function of PSF1 in G_2-M progression. In the scrambled shRNA–treated control population, most cells had divided within 60 minutes, whereas division times were prolonged in the PSF1-depleted cells (Fig. 6D, left). To examine this in terms of chromosome segregation, real-time imaging was done with histone H2B-GFP, which labels the chromosomes (Fig. 6D, middle). In control cells, the chromosomes were condensed and congressed to the metaphase plate, but subsequently, and suddenly, they completely segregated and the

time spent in metaphase was between 15 and 30 minutes. By contrast, PSF1 depletion prolonged the duration of metaphase by between 33 and 145 minutes, and a proportion of the PSF1-depleted cells showed abnormal chromosome congression and segregation (data not shown). Real-time observation with GFP-tubulin also revealed that depletion of PSF1 caused arrest at metaphase (data not shown). To resolve whether this mitotic arrest, induced by PSF1 depletion, was dependent on the spindle assembly checkpoint, Mad2 was co-depleted from the cells. We found that the mitotic arrest of almost all co-depleted cells was rescued by the early onset of anaphase (Fig. 6D, right). Taken together, these data showed that, in the absence of PSF1, the spindle checkpoint signal was activated and mitotic arrest was precipitated.

Because we observed abnormalities in metaphase arrest and DNA segregation in PSF1-depleted cells, we next analyzed spindle organization by staining for β-tubulin. Results showed that approximately 10% of the mitotic cells formed multipolar asters (Fig. 6E, left), whereas a small number of abnormal spindles were found in the control experiments (data not shown). Moreover, by immunostaining with anti-survivin antibody, we found that unaligned chromosomes were present in PSF1 shRNA–treated cells, which may reflect a defect in chromosome congression or segregation (Fig. 6E, middle). Recently, we reported that PSF1-deficient mice were nonviable at around embryonic day E6.5 and that BrdUrd incorporation was inhibited in the cultured inner cell mass from the blastocysts of E3.5 *PSF1*$^{-/-}$ embryos (12). Consistent with the present results from RNAi experiments in HeLa cells, we found that micronuclei and abnormal chromosomal segregation occurred in E3.5 *PSF1*$^{-/-}$ blastocysts (Fig. 6E, right). These data indicate that PSF1 contributes not only

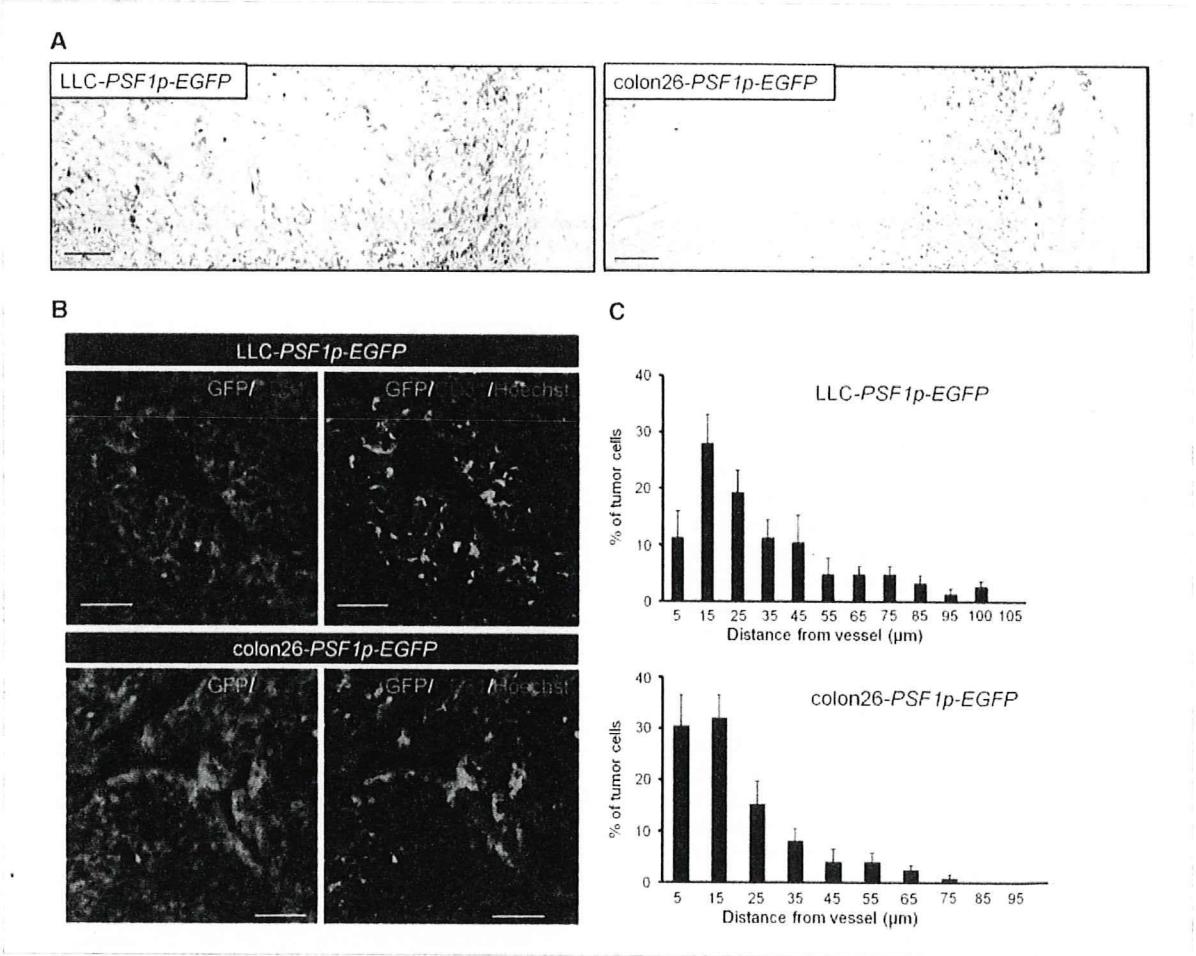

Figure 5. Localization of cancer cells strongly expressing PSF1. A, sections from LLC-*PSF1p-EGFP* (left) and colon26-*PSF1p-EGFP* (right) xenografts were double stained with anti-GFP antibody (brown in left, purple in right) and anti-CD31 antibody (red). Bar, 100 μm. B, sections of LLC-*PSF1p-EGFP* (top) and colon26-*PSF1p-EGFP* (bottom) tumor tissues were stained with anti-CD31 antibody (red). Nuclei were counterstained with Hoechst 33342 (blue). Endogenous EGFP was observed in low contrast (left) and high contrast (right). C, percentages of EGFP^{high} cells that were located at incremental distances of 5 μm from the nearest CD31^{+} endothelial cells. Data are mean ± SEM from five random fields. Bar, 100 μm.

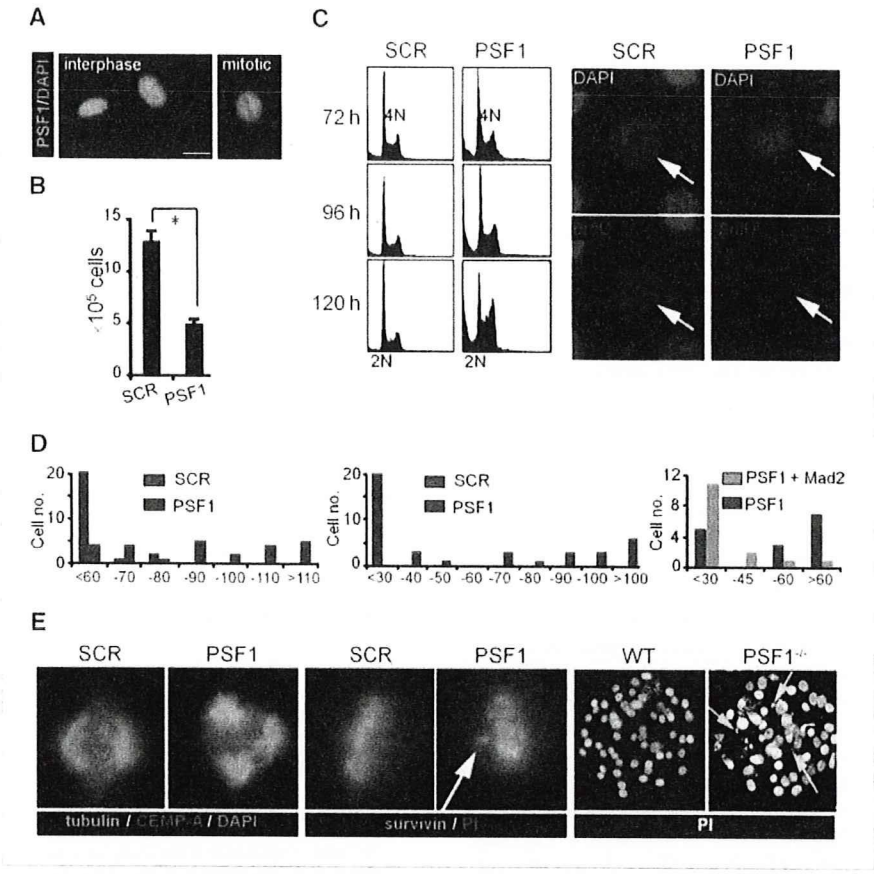

Figure 6. *PSF1* silencing inhibits proliferation of cancer cells. A, HeLa cells were immunostained with anti-PSF1 (green). DNA was counterstained with 4',6-diamidino-2-phenylindole (DAPI; blue). B, total numbers of RNAi-treated HeLa cells 96 h after transfection (bottom). *SCR*, nonspecific scrambled shRNA as a negative control. *, $P < 0.05$. C, DNA content of shRNA-treated HeLa cells (72 h after transfection) was determined by flow cytometry (left). DNA synthesis in large nucleated cells treated with the indicated shRNA. Immunostaining was done with anti-BrdUrd antibody (red), and counterstaining with DAPI (blue; right). Arrows, large nuclei. D, HeLa cells were treated with control (blue) or PSF1 (red) shRNA. Time required for cell division was evaluated by time-lapse observation 72 to 96 h after transfection (left). Using histone H3-GFP–expressing HEK293T cells, metaphase retention time was observed 72 to 120 h after transfection (middle). The H3-GFP-HEK293T cells were cotransfected with PSF1 shRNA and scrambled shRNA (red) or PSF1 and Mad2 shRNA vectors (green), and metaphase retention time was observed 36 to 72 h after transfection (right). E, HeLa cells transfected with shRNA as indicated. Expression of tubulin (green) and CENP-A (red; left). DNA was counterstained with DAPI (blue). Expression of survivin (green; middle). DNA was counterstained with propidium iodide (red). E3.5 $PSF1^{+/+}$ or $PSF1^{-/-}$ embryos were fixed and stained with propidium iodide (right). Arrows, disorganized micronuclei.

to DNA replication but also to the transition from metaphase to anaphase, as well as to chromosome segregation.

Discussion

In the present work, we used cells with a high level of expression of PSF1 to show that these malignant cancer cells, which are located in the vascular region and at the edge of the tumor, exhibit high tumorigenic and metastatic ability.

Thus far, acquisition of genetic changes affected by epigenetic manipulation and microenvironmental exposure has been suggested to be responsible for tumor progression. When we cultured the tumor cells *in vitro*, we observed that the population consisted of PSF1(EGFP)^{high} and PSF1(EGFP)^{low} fractions. When sorted and separately injected into mice, we failed to detect any marked differences between them in terms of tumorigenic or metastatic capacity (data not shown). When nonfractionated tumor cells from these cultures were injected, the tumors that developed consisted of both PSF1(EGFP)^{high} and PSF1(EGFP)^{low} cells. However, when these cells extracted from tumors *in vivo* were fractionated into PSF1(EGFP)^{high} and PSF1(EGFP)^{low} and injected into mice again, then we did see clear a difference in terms of tumorigenic and metastatic capacity between the two fractions.

Our model therefore strongly supports the possibility that environmental changes *in vivo* clearly affect the features of cancer cells with regard to tumorigenicity or nontumorigenicity. Thus, this model suggested that the interaction of cancer

cells with their microenvironment changes them into more malignant ones. In our tumor model as well as histology of human tissues, cells highly positive for PSF1 are located near blood vessels. It has been suggested that CSCs/CICs localize in the perivascular region (26), as is observed in normal organs, where stem cells are located in the vascular niche (27). Furthermore, microarray data clearly indicated that ESC-like signatures, which are reported to be enriched in CSCs/CICs fractions, were also enriched in $EGFP^{high}$ cells versus $EGFP^{low}$ cells (Fig. 4). Thus, the subpopulation of cells strongly positive for PSF1 might include the CSC/CIC fraction.

Antitumor angiogenesis is a promising approach for managing cancer patients, and many angiogenesis-disrupting agents have been developed (28). Although some agents have already been tested clinically and prolongation of survival has been confirmed, it is impossible to destroy all of the blood vessels in a tumor. Recent research in mice has suggested that the tumor repopulates from the edge region to the center after treatment with an angiogenesis-disrupting agent (28), and also that malignant tumor cells egress through remnant blood vessels at the tumor edge after inhibition of vascular endothelial growth factor signals (29). We previously reported that blood vessels in peripheral regions of tumors are well matured compared with those in the center and that they are resistant to antiangiogenic drugs (19, 30). Our data therefore strongly support the notion that cells with malignant features located near blood vessels at the tumor edge and showing resistance to angiogenesis-disrupting agents are responsible for invasion and metastasis. Our present model represents a precise analytic tool to determine whether candidate drugs directed against cells with malignant features including CSCs/CICs or blood vessels actually do suppress proliferation of cancer cells or destroy the vascular niche.

Our data clearly indicate that PSF1 plays a pivotal role in DNA replication and microtubule organization. Recently, it has been suggested that molecules homologous with those associated with DNA replication in lower species also regulate other cellular events in mammalian cells (31–33). In higher eukaryotes, a number of environmental cues affecting cell division involve DNA replication proteins that are also used by lower eukaryotes and that perform diverse functions in cytokinesis. Therefore, there is a possibility that, in addition to its role in microtubule organization, which we have shown here, plus the known part it plays in DNA replication, PSF1 may also have other cellular functions in symmetrical or asymmetrical cell division of malignant cancer cells by influencing cell structure. As we showed here, the possibility that PSF1 is expressed by malignant cancer cells, which may include CSCs or CICs, and the finding that silencing PSF1 induced cancer cell apoptosis suggest that this molecule may represent an important new target for the development of anticancer drugs.

Disclosure of Potential Conflicts of Interest

No potential conflicts of interest were disclosed.

Acknowledgments

We thank N. Fujimoto and K. Fukuhara for technical assistance, and A. Taguchi for technical assistance with the microarray analysis.

Grant Support

Japanese Ministry of Education, Culture, Sports, Science and Technology and the Japanese Society for Promotion of Science.

The costs of publication of this article were defrayed in part by the payment of page charges. This article must therefore be hereby marked *advertisement* in accordance with 18 U.S.C. Section 1734 solely to indicate this fact.

Received 10/7/09; revised 11/25/09; accepted 12/3/09; published OnlineFirst 1/26/10.

References

1. Takayama Y, Kamimura Y, Okawa M, Muramatsu S, Sugino A, Araki H. GINS, a novel multiprotein complex required for chromosomal DNA replication in budding yeast. Genes Dev 2003;17:1153–65.
2. Bauerschmidt C, Pollok S, Kremmer E, Nasheuer HP, Grosse F. Interactions of human Cdc45 with the Mcm2-7 complex, the GINS complex, and DNA polymerases δ and epsilon during S phase. Genes Cells 2007;12:745–58.
3. Gambus A, Jones RC, Sanchez-Diaz A, et al. GINS maintains association of Cdc45 with MCM in replisome progression complexes at eukaryotic DNA replication forks. Nat Cell Biol 2006;8:358–66.
4. Kanemaki M, Sanchez-Diaz A, Gambus A, Labib K. Functional proteomic identification of DNA replication proteins by induced proteolysis *in vivo*. Nature 2003;423:720–4.
5. Moyer SE, Lewis PW, Botchan MR. Isolation of the Cdc45/Mcm2-7/GINS (CMG) complex, a candidate for the eukaryotic DNA replication fork helicase. Proc Natl Acad Sci U S A 2006;103:10236–41.
6. Pacek M, Tutter AV, Kubota Y, Takisawa H, Walter JC. Localization of MCM2-7, Cdc45, and GINS to the site of DNA unwinding during eukaryotic DNA replication. Mol Cell 2006;21:581–7.
7. Chang YP, Wang G, Bermudez V, Hurwitz J, Chen XS. Crystal structure of the GINS complex and functional insights into its role in DNA replication. Proc Natl Acad Sci U S A 2007;104:12685–90.
8. De Falco M, Ferrari E, De Felice M, Rossi M, Hubscher U, Pisani FM. The human GINS complex binds to and specifically stimulates human DNA polymerase α-primase. EMBO Rep 2007;8:99–103.
9. Kamada K, Kubota Y, Arata T, Shindo Y, Hanaoka F. Structure of the human GINS complex and its assembly and functional interface in replication initiation. Nat Struct Mol Biol 2007;14:388–96.
10. Kubota Y, Takase Y, Komori Y, et al. A novel ring-like complex of *Xenopus* proteins essential for the initiation of DNA replication. Genes Dev 2003;17:1141–52.
11. Barkley LR, Song IY, Zou Y, Vaziri C. Reduced expression of GINS complex members induces hallmarks of pre-malignancy in primary untransformed human cells. Cell Cycle 2009;8:1577–88.
12. Ueno M, Itoh M, Kong L, Sugihara K, Asano M, Takakura N. PSF1 is essential for early embryogenesis in mice. Mol Cell Biol 2005;25:10528–32.
13. Han Y, Ueno M, Nagahama Y, Takakura N. Identification and characterization of stem cell-specific transcription of PSF1 in spermatogenesis. Biochem Biophys Res Commun 2009;380:609–13.
14. Ueno M, Itoh M, Sugihara K, Asano M, Takakura N. Both alleles of

PSF1 are required for maintenance of pool size of immature hematopoietic cells and acute bone marrow regeneration. Blood 2009; 113:555–62.
15. Obama K, Ura K, Satoh S, Nakamura Y, Furukawa Y. Up-regulation of PSF2, a member of the GINS multiprotein complex, in intrahepatic cholangiocarcinoma. Oncol Rep 2005;14:701–6.
16. Hayashi R, Arauchi T, Tategu M, Goto Y, Yoshida K. A combined computational and experimental study on the structure-regulation relationships of putative mammalian DNA replication initiator GINS. Genomics Proteomics Bioinformatics 2006;4:156–64.
17. Ryu B, Kim DS, Deluca AM, Alani RM. Comprehensive expression profiling of tumor cell lines identifies molecular signatures of melanoma progression. PLoS One 2007;2:e594.
18. Ben-Porath I, Thomson MW, Carey VJ, et al. An embryonic stem cell-like gene expression signature in poorly differentiated aggressive human tumors. Nat Genet 2008;40:499–507.
19. Satoh N, Yamada Y, Kinugasa Y, Takakura N. Angiopoietin-1 alters tumor growth by stabilizing blood vessels or by promoting angiogenesis. Cancer Sci 2008;99:2373–9.
20. Kanda T, Sullivan KF, Wahl GM. Histone-GFP fusion protein enables sensitive analysis of chromosome dynamics in living mammalian cells. Curr Biol 1998;8:377–85.
21. Fujita H, Fukuhara S, Sakurai A, et al. Local activation of Rap1 contributes to directional vascular endothelial cell migration accompanied by extension of microtubules on which RAPL, a Rap1-associating molecule, localizes. J Biol Chem 2005;280:5022–31.
22. Fukuhara S, Sako K, Minami T, et al. Differential function of Tie2 at cell-cell contacts and cell-substratum contacts regulated by angiopoietin-1. Nat Cell Biol 2008;10:513–26.
23. Subramanian A, Tamayo P, Mootha VK, et al. Gene set enrichment analysis: a knowledge-based approach for interpreting genome-wide expression profiles. Proc Natl Acad Sci U S A 2005;102:15545–50.
24. Wong DJ, Liu H, Ridky TW, Cassarino D, Segal E, Chang HY. Module map of stem cell genes guides creation of epithelial cancer stem cells. Cell Stem Cell 2008;2:333–44.
25. Somervaille TC, Matheny CJ, Spencer GJ, et al. Hierarchical maintenance of MLL myeloid leukemia stem cells employs a transcriptional program shared with embryonic rather than adult stem cells. Cell Stem Cell 2009;4:129–40.
26. Calabrese C, Poppleton H, Kocak M, et al. A perivascular niche for brain tumor stem cells. Cancer Cell 2007;11:69–82.
27. Kiel MJ, Yilmaz OH, Iwashita T, Terhorst C, Morrison SJ. SLAM family receptors distinguish hematopoietic stem and progenitor cells and reveal endothelial niches for stem cells. Cell 2005;121:1109–21.
28. Tozer GM, Kanthou C, Baguley BC. Disrupting tumour blood vessels. Nat Rev Cancer 2005;5:423–35.
29. Paez-Ribes M, Allen E, Hudock J, et al. Antiangiogenic therapy elicits malignant progression of tumors to increased local invasion and distant metastasis. Cancer Cell 2009;15:220–31.
30. Okamoto R, Ueno M, Yamada Y, et al. Hematopoietic cells regulate the angiogenic switch during tumorigenesis. Blood 2005;105: 2757–63.
31. Kearsey SE, Cotterill S. Enigmatic variations: divergent modes of regulating eukaryotic DNA replication. Mol Cell 2003;12:1067–75.
32. Hemerly AS, Prasanth SG, Siddiqui K, Stillman B. Orc1 controls centriole and centrosome copy number in human cells. Science 2009; 323:789–93.
33. Prasanth SG, Prasanth KV, Stillman B. Orc6 involved in DNA replication, chromosome segregation, and cytokinesis. Science 2002;297: 1026–31.

Biochemical and Biophysical Research Communications 392 (2010) 150–154

Contents lists available at ScienceDirect

Biochemical and Biophysical Research Communications

journal homepage: www.elsevier.com/locate/ybbrc

PSF3 marks malignant colon cancer and has a role in cancer cell proliferation

Yumi Nagahama [a], Masaya Ueno [a,b], Naotsugu Haraguchi [c], Masaki Mori [c], Nobuyuki Takakura [a,*]

[a] Department of Signal Transduction, Research Institute for Microbial Diseases, Osaka University, 3-1 Yamadaoka, Suita, Osaka 565-0871, Japan
[b] Department of Molecular, Cell and Developmental Biology, University of California, Los Angeles, CA 90095, USA
[c] Department of Gastroenterological Surgery, Graduate School of Medicine, Osaka University, 2-2 Yamadaoka, Suita, 565-0871, Japan

ARTICLE INFO

Article history:
Received 22 December 2009
Available online 6 January 2010

Keywords:
PSF3
Colon carcinoma

ABSTRACT

PSF3 (partner of Sld five 3) is a member of the tetrameric complex termed GINS, composed of SLD5, PSF1, PSF2, and PSF3, and well-conserved evolutionarily. Previous studies suggested that some GINS complex members are upregulated in cancer, but PSF3 expression in colon carcinoma has not been investigated. Here, we established a mouse anti-PSF3 antibody, and examined PSF3 expression in human colon carcinoma cell lines and colon carcinoma specimens. We found that PSF3 is expressed in the crypt region in normal colonic mucosa and that many PSF3-positive cells co-expressed Ki-67. This suggests that PSF3-positivity of normal mucosa is associated with cell proliferation. Expression of the PSF3 protein was greater in carcinoma compared with the adjacent normal mucosa, and even stronger in high-grade malignancies, suggesting that it may be associated with colon cancer progression. PSF3 gene knock-down in human colon carcinoma cell lines resulted in growth inhibition characterized by delayed S-phase progression. These results suggest that PSF3 is a potential biomarker for diagnosis of progression in colon cancer and could be a new target for cancer therapy.

Introduction

PSF3 (partner of Sld five 3) is a member of the highly evolutionarily conserved tetrameric complex termed GINS, composed of SLD5, PSF1, PSF2, and PSF3. In yeast, the GINS complex associates with the Minichromosome maintenance (MCM) 2–7 complex and with CDC45, and this "C–M–G complex" (CDC45–MCM–2–7–GINS) regulates both the initiation and progression of DNA replication [1–6]. Thus, it has been suggested that GINS is involved in DNA replication in *Xenopus* and human [7–10]. However, a recent study suggested that PSF1/2 is associated with the response to replication stress and acquisition of DNA damage in untransformed human dermal fibroblasts [11]. As it has been reported that DNA replication-associated protein in yeast has diverse functions in different cells, e.g. origin recognition protein Orc1 has a role in determining centrosome copy number [12], the exact functions of GINS components in mammalian cells are not yet clear.

We have previously cloned the mouse ortholog of *PSF1* (partner of SLD5) from a hematopoietic stem cell (HSC) cDNA library [13] and found that *PSF1* expression in mice was predominantly observed in the adult BM and thymus, as well as the testis and ovary, i.e. tissues in which stem cell proliferation is actively induced and continues after birth. Moreover, we reported that PSF1 is strongly expressed in several immature cell lineages such as cells in the inner cell mass during early embryogenesis, and spermatogonia as well as HSCs after birth [13–15]. Loss of *PSF1* led to embryonic lethality around the implantation stage caused by the inability of cells of the inner cell mass to proliferate [13]. Moreover, haploinsufficiency of PSF1 in $PSF1^{+/-}$ mice resulted in the delayed induction of HSC proliferation during reconstitution of bone marrow after 5-FU ablation. These data strongly suggested that PSF1 is required for acute proliferation of cells, especially immature cells such as stem cells and progenitor cells. However, the role of the other components of GINS in mammalian cells has not been well determined.

Several recent reports have suggested a role for GINS components in cancer cells. For example, all GINS components were found to be overexpressed in intrahepatic cholangiocarcinoma tissues [16]. In a Gene Expression Omnibus (GEO) database search, *PSF1* was identified as an estrogen target in MCF7 human breast carcinoma cells [17]. In a comprehensive study, it was found that *PSF1* and *SLD5* were upregulated in aggressive melanoma [18].

Although several studies have suggested that GINS components play a role in cancer as described above, their expression in colon carcinoma has not been examined. Among the GINS complex members, the expression and role of PSF3 has not been well-documented because no appropriate antibody was available thus far. Therefore, we generated such an antibody against PSF3 and

Abbreviations: GINS, Go-ichi-ni-san; PSF, Partner of Sld five.

* Corresponding author. Fax: +81 6 6879 8314.
E-mail address: ntakaku@biken.osaka-u.ac.jp (N. Takakura).

0006-291X/$ - see front matter © 2010 Elsevier Inc. All rights reserved.
doi:10.1016/j.bbrc.2009.12.174

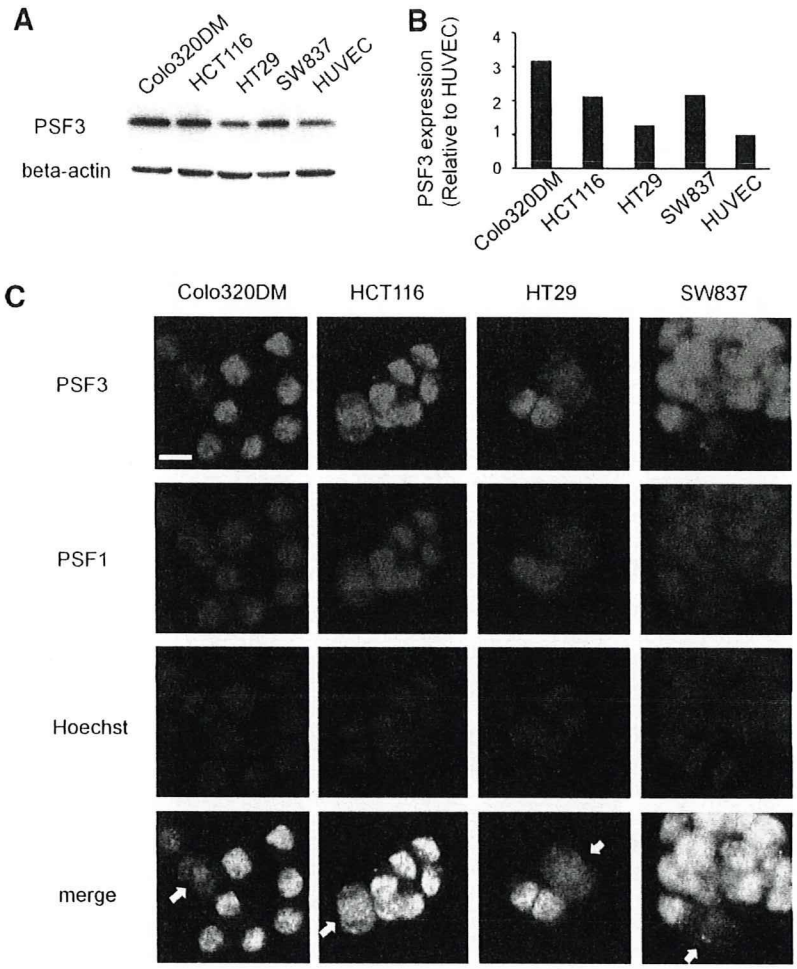

Fig. 1. PSF3 expression in human colon carcinoma cell lines. (A,B) Western blotting of PSF3 expression in whole cell extracts of each cell line as indicated. A representative result of Western blotting (A) and densitometric analysis for quantitative evaluation (B) are shown. (C) Cells as indicated were stained with anti-PSF3 antibody labeled with Alexa488 (green) and co-stained with anti-PSF1 antibody labeled with Cy3 (red). DNA was counter-stained with Hoechst (blue). Arrows, mitotic cells. Bar, 10 μm.

examined its reactivity with human colon carcinoma specimens. Furthermore, we silenced the *PSF3* gene by RNAi methodology to determine the impact of PSF3 knock-down on the growth of human colon carcinoma cell lines.

Materials and methods

Generation of anti-PSF3 antibody. For the generation of monoclonal anti-PSF3 antibody, PSF3 cDNA, coding full-length amino acid residues, was amplified by polymerase chain reaction (PCR), and then DNA fragments were ligated into pGEX-2T vector (Pharmacia Piscataway, NJ) for the preparation of glutathione *S*-transferase (GST)-fusion proteins. Purified GST-fused protein was used as antigen for mouse immunization, and hybridoma cells were established by standard procedures. Finally, stable hybridoma cell lines were obtained and cloned as aps3.2 and aps3.14. In this current study, aps3.2 was used. The specificities of the antibodies were analyzed by Western blotting and immunocytochemistry.

Cell lines. HCT116, colo320DM, SW837, HT-29 were maintained in RPMI medium (Sigma, St. Louis, MO) with 10% fetal bovine serum (FBS) (Sigma) and penicillin/streptomycin (GIBCO, Rockville, MD). Human umbilical vein endothelial cells (HUVECs) were maintained in HuMedia EG2 (Kurabo, Osaka, Japan).

Western blotting. Total cell lysates were heated for 3 min at 95 °C and then loaded onto SDS–polyacrylamide gels. Proteins were electrophoretically transferred onto polyvinylidene difluoride membranes (Millipore, MA, USA), blocked with 5% nonfat dry milk, then blotted with anti-PSF3 antibody or anti-beta actin antibody (Sigma). Blots were developed with peroxidase-labeled anti-mouse Ig antibodies (Dako, Carpinteria, CA) using enhanced chemiluminescence (ECL detection system; Amersham, Buckinghamshire, UK).

Immunocytochemistry. For staining of PSF1 and PSF3, 4% PFA in phosphate buffer saline (PBS) and cold methanol was used for fixations. Following three washes with PBS, cells were incubated with anti-PSF1 [15] and anti-PSF3 antibody, then washed with PBS and incubated with goat anti-mouse IgG Alexa488 (for PSF3, Invitrogen, Carlsbad, CA, USA) or anti-rat IgG Biotin (for PSF1, Invitrogen) followed by Streptavidin-Cy3 (Zymed). Nuclear DNA was counterstained with Hoechst (Sigma).

Immunohistochemistry. For human specimens, immnohistochemistry was performed on formalin-fixed, paraffin-embedded tumor samples. All specimens were obtained from the Department of Gastroenterological Surgery, Graduate School of Medicine, Osaka University. For the immunohistochemical analyses, mouse anti-PSF3 antibody (aps3.2) or anti-Ki-67 antibody (Dako) was used for primary antibodies. As a secondary antibody for anti-PSF3 or anti-Ki-67 antibody, Biotin-conjugated goat anti-mouse Ig (Dako) was used. After washing the slides three times with 0.05% Triton X-100 in PBS, they are incubated with VECSTAIN ABC Standard

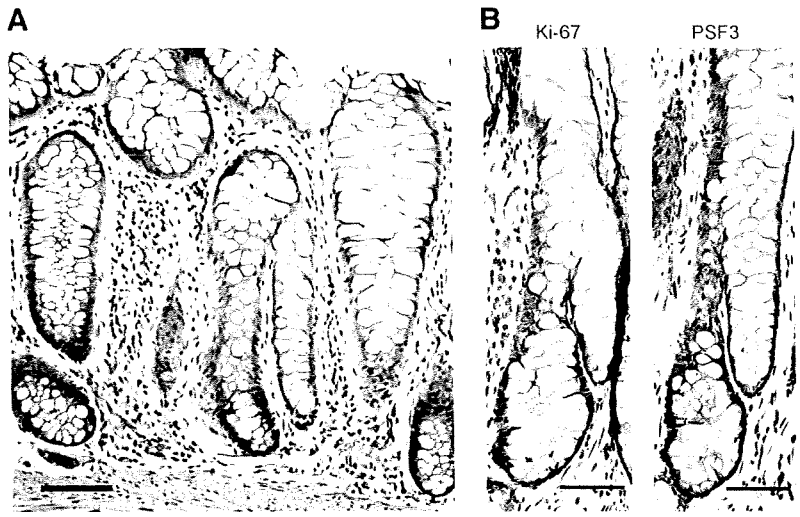

Fig. 2. PSF3 expression in human colonic mucosa. (A) Immunohistochemical analysis of PSF3 (brown) expression in human colonic mucosa. Bar, 100 μm. (B) Immunohistochemical analysis of Ki-67 (brown) and PSF3 (brown) expression in serial sections of human colon mucosa. Bars, 50 μm.

Kit (Vector Laboratories, Burlingame, CA, USA). For the visualization of HRP, diaminobenzidine (Dojindo, Kumamoto, Japan) was used. The slides were counter-stained with hematoxylin.

RNA interference. Small interfering RNA (siRNA) specific to human PSF3 and negative control siRNA were purchased from Invitrogen. The effect of siRNA transfection was optimized using RNAiMAX (Invitrogen) according to the manufacturer's protocol. The effect of siRNA on PSF3 expression was observed using Western blotting with an anti-PSF3 antibody. Cell numbers were counted by a hemocytometer.

BrdU-FACS. For BrdU detection, 10 μM BrdU was added to the medium for 15 min prior to cell collection. Cells were fixed in 70% ethanol and washed in PBS, treated with 1 N HCl for 30 min and incubated with anti-BrdU antibody (BD Bioscience Pharmingen, SanDiego, USA), followed by anti-mouse IgG Alexa488 (Invitrogen).

Results

PSF3 expression in human colon carcinoma cell lines

We compared the expression of PSF3 in human colon carcinoma cell lines and non-tumor cells (HUVECs). Overall, tumor cells expressed higher levels of PSF3 protein than HUVECs (Fig. 1A and B). Next, we performed immunocytochemistry to localize PSF3 in colon carcinoma cells. Nuclear accumulation of PSF3 was observed during interphase, whereas during mitosis, it was almost exclusively located outside the chromatin with a diffuse pattern

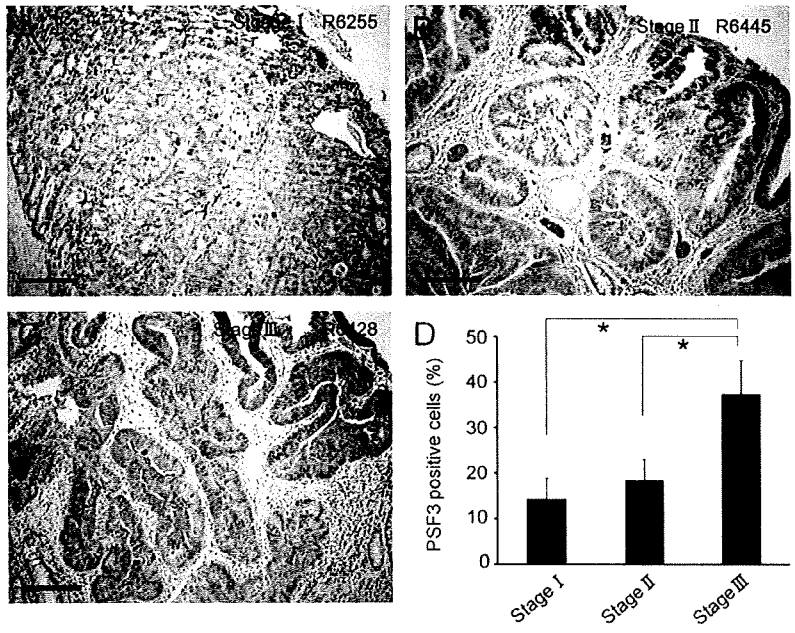

Fig. 3. PSF3 expression in human colon carcinoma specimens. (A–C) PSF3 (brown) expression in human colon carcinoma specimens in different stages (A, stage I; B, stage II; C, stage III). Bars, 200 μm. (D) Percentages of tumor cells that are PSF3-positive. *$P < 0.05$ ($n = 6$, mean ± SEM).

(Fig. 1C). These characteristics are similar to PSF1, one of the other GINS components (Fig. 1C), suggesting colocalization of PSF3 and PSF1 as a GINS component in human colon carcinoma cells.

PSF3 expression in human normal colonic mucosa and colon carcinoma specimens

Several studies have suggested that GINS components play a role in tumor progression [16–18]. To test whether PSF3 may also be involved in human colon cancer progression, its expression in colon carcinoma pathological specimens was investigated using immunohistochemistry.

In adjacent normal large bowel mucosa, PSF3 expression was confined to the base of the colon crypts, which corresponds to the proliferative zone of the mucosa (Fig. 2A). Using serial tissue sections, we compared expression of PSF3 with Ki-67, a marker of proliferation. The majority of PSF3-positive cells was found to co-express Ki-67 (Fig. 2B), indicating cell cycling. Our previous study showed that PSF1 is also expressed in crypt base columnar cells and that the number of such cells decreased in adult haploinsufficient *PSF1*$^{+/-}$ mice compared with adult wild-type mice [15]. Based on these results, we suggest that the GINS complex may play an important role in proliferation of colon crypt cells.

Additionally, in colon carcinoma specimens from patients, higher levels of expression of PSF3 protein were found in the cancer cells than the adjacent normal mucosa. Moreover, the percentage of PSF3-positive cancer cells correlated positively with the stage of cancer (Fig. 3). This further suggests that PSF3 protein expression associates with colon cancer progression.

PSF3 knock-down results in growth arrest of human colon carcinoma cells

To assess whether PSF3 is involved in colon cancer cell proliferation, we evaluated the silencing effect of PSF3 on cell growth using RNAi methodology to target three different coding regions of the human *PSF3* mRNA sequence. The efficiency of *PSF3* knockdown was examined by Western blotting, indicating that PSF3 protein expression in both HCT116 and colo320DM cells was greatly attenuated, in particular by two different sequences (siPSF3-2, 3) (Fig. 4A). PSF3 knock-down in either cell line resulted in inhibition of proliferation (Fig. 4B). This inhibitory effect correlated with PSF3 expression silencing efficiency, because less effects on cell proliferation were observed with siPSF3-1. The relationship of cell cycling to reduction of PSF3 expression was assessed by the incorporation of nucleotide analogues. Results indicated that attenuation of PSF3

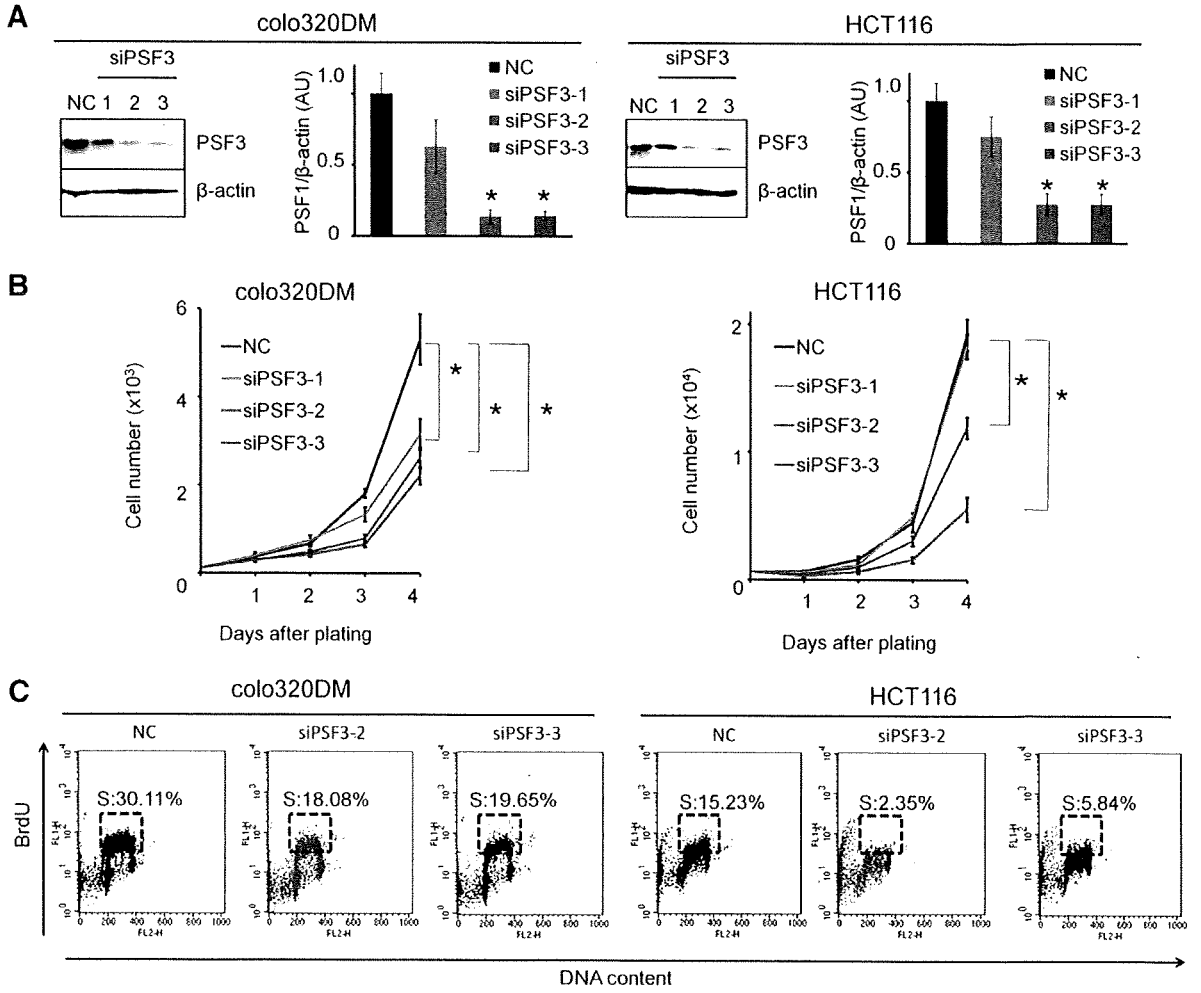

Fig. 4. PSF3 knock-down results in growth inhibition in colon carcinoma cell lines. (A) Western blotting for PSF3 expression after silencing by three RNAis (siPSF3-1, 2 and 3) or a control RNAi (NC). Densitometric analysis was performed for quantitative evaluation ($n = 4$). *$P < 0.05$ vs control. (B) Cell growth after introduction of RNAi as described in (A). *$P < 0.05$ ($n = 8$, mean ± SEM). (C) Cellular BrdU incorporation assay was carried out 48 h after transfection with the indicated siRNA. BrdU was incorporated for 15 min. BrdU intensity is represented in the logarithmic *y*-axis and DNA content on the linear *x*-axis. Gates define the percentage of cells in S-phase.

expression reduced the percentage of cells in S-phase (Fig. 4C). Thus, we conclude that PSF3 plays a role in cell cycling, especially S-phase progression.

Discussion

In this study, we found high levels of expression of PSF3 in several colon carcinoma cell lines and overexpression of PSF3 in stage-matched human colon cancer cells from higher grade tumors. Our preliminary experiments showed that PSF3 is more highly expressed in cancer cells invading into muscle than in non-invasive cancer (data not shown). It has been reported that several prereplicative complex proteins are overexpressed in cancer and serve as good tumor markers [19]. For example, MCM-2 (a member of the C–M–G complex) was reported to be significantly associated with Dukes' stage, existence of lymph node metastasis, tumor histological grade, presence of malignancy in adenoma, and venous invasion in colon cancer [20]. Based on these findings, our present data suggest that PSF3 might be a potential biomarker for diagnosis of progression and during the initiation of metastasis in colon cancer. Comparison of PSF3 with other proliferation markers, such as Ki-67 and PCNA, might support this hypothesis.

Previous studies have shown that DNA replication factors, including GINS, are differently expressed in *Xenopus*, suggesting that different factors are utilized in different developmental regions [21]. Further studies of precise expression profiles and functions of individual GINS components in mammalian tissues might help us to understand how such individual components are involved in tumor growth occurring in a wide variety of tissues and organs. Here, we documented PSF3 expression in the base of the crypts in normal colon and found that PSF3 expression was co-localized with PSF1 in human colon carcinoma cell lines. Moreover, PSF3 knock-down resulted in growth inhibition of colon cancer cells by the suppression of S-phase progression, indicating that PSF3 acts at least as a GINS complex and is essential for S-phase progression in human colon carcinoma cells. Further studies are required to elucidate the contributions of individual GINS components in the growth of other tumors.

Several studies have indicated that pre-RC proteins may potentially have significant therapeutic value [19]. Interestingly, Orc6, one such pre-RC protein, was reported to be associated with 5-fluorouracil (5-FU) resistance in human colon cancer cell lines [22], and its downregulation sensitized colon cancer cells to 5-FU and cisplatin [23]. These results suggest that pre-RC proteins may play a role in chemoresistance. Based on these reports, our data suggest that PSF3 might be a potential therapeutic target as well as a potential diagnosis marker for colon carcinoma.

Acknowledgments

We are grateful to N. Fujimoto and K. Fukuhara for technical assistance. This work was partly supported by the Japanese Ministry of Education, Culture, Sports, Science and Technology and the Japanese Society for Promotion of Science.

References

[1] Y. Takayama, Y. Kamimura, M. Okawa, S. Muramatsu, A. Sugino, H. Araki, GINS, a novel multiprotein complex required for chromosomal DNA replication in budding yeast, Genes Dev. 17 (2003) 1153–1165.
[2] C. Bauerschmidt, S. Pollok, E. Kremmer, H.P. Nasheuer, F. Grosse, Interactions of human Cdc45 with the Mcm2–7 complex, the GINS complex, and DNA polymerases delta and epsilon during S phase, Genes Cells 12 (2007) 745–758.
[3] A. Gambus, R.C. Jones, A. Sanchez-Diaz, et al., GINS maintains association of Cdc45 with MCM in replisome progression complexes at eukaryotic DNA replication forks, Nat. Cell Biol. 8 (2006) 358–366.
[4] M. Kanemaki, A. Sanchez-Diaz, A. Gambus, K. Labib, Functional proteomic identification of DNA replication proteins by induced proteolysis in vivo, Nature 423 (2003) 720–724.
[5] S.E. Moyer, P.W. Lewis, M.R. Botchan, Isolation of the Cdc45/Mcm2–7/GINS (CMG) complex, a candidate for the eukaryotic DNA replication fork helicase, Proc. Natl. Acad. Sci. USA 103 (2006) 10236–10241.
[6] M. Pacek, A.V. Tutter, Y. Kubota, H. Takisawa, J.C. Walter, Localization of MCM2–7, Cdc45, and GINS to the site of DNA unwinding during eukaryotic DNA replication, Mol. Cell 21 (2006) 581–587.
[7] Y.P. Chang, G. Wang, V. Bermudez, J. Hurwitz, X.S. Chen, Crystal structure of the GINS complex and functional insights into its role in DNA replication, Proc. Natl. Acad. Sci. USA 104 (2007) 12685–12690.
[8] M. De Falco, E. Ferrari, M. De Felice, M. Rossi, U. Hubscher, F.M. Pisani, The human GINS complex binds to and specifically stimulates human DNA polymerase alpha-primase, EMBO Rep. 8 (2007) 99–103.
[9] K. Kamada, Y. Kubota, T. Arata, Y. Shindo, F. Hanaoka, Structure of the human GINS complex and its assembly and functional interface in replication initiation, Nat. Struct. Mol. Biol. 14 (2007) 388–396.
[10] Y. Kubota, Y. Takase, Y. Komori, et al., A novel ring-like complex of *Xenopus* proteins essential for the initiation of DNA replication, Genes Dev. 17 (2003) 1141–1152.
[11] L.R. Barkley, I.Y. Song, Y. Zou, C. Vaziri, Reduced expression of GINS complex members induces hallmarks of pre-malignancy in primary untransformed human cells, Cell Cycle 8 (2009) 1577–1588.
[12] A.S. Hemerly, S.G. Prasanth, K. Siddiqui, B. Stillman, Orc1 controls centriole and centrosome copy number in human cells, Science 323 (2009) 789–793.
[13] M. Ueno, M. Itoh, L. Kong, K. Sugihara, M. Asano, N. Takakura, PSF1 is essential for early embryogenesis in mice, Mol. Cell. Biol. 25 (2005) 10528–10532.
[14] Y. Han, M. Ueno, Y. Nagahama, N. Takakura, Identification and characterization of stem cell-specific transcription of PSF1 in spermatogenesis, Biochem. Biophys. Res. Commun. 380 (2009) 609–613.
[15] M. Ueno, M. Itoh, K. Sugihara, M. Asano, N. Takakura, Both alleles of PSF1 are required for maintenance of pool size of immature hematopoietic cells and acute bone marrow regeneration, Blood 113 (2009) 555–562.
[16] K. Obama, K. Ura, S. Satoh, Y. Nakamura, Y. Furukawa, Up-regulation of PSF2, a member of the GINS multiprotein complex, in intrahepatic cholangiocarcinoma, Oncol. Rep. 14 (2005) 701–706.
[17] R. Hayashi, T. Arauchi, M. Tategu, Y. Goto, K. Yoshida, A combined computational and experimental study on the structure-regulation relationships of putative mammalian DNA replication initiator GINS, Genomics Proteomics Bioinformatics 4 (2006) 156–164.
[18] B. Ryu, D.S. Kim, A.M. Deluca, R.M. Alani, Comprehensive expression profiling of tumor cell lines identifies molecular signatures of melanoma progression, PLoS One 2 (2007) e594.
[19] E. Lau, T. Tsuji, L. Guo, S.H. Lu, W. Jiang, The role of pre-replicative complex (pre-RC) components in oncogenesis, FASEB J. 21 (2007) 3786–3794.
[20] C. Giaginis, M. Georgiadou, K. Dimakopoulou, et al., Clinical significance of MCM-2 and MCM-5 expression in colon cancer: association with clinicopathological parameters and tumor proliferative capacity, Dig. Dis. Sci. 54 (2009) 282–291.
[21] B.E. Walter, J.J. Henry, Embryonic expression of pre-initiation DNA replication factors in *Xenopus laevis*, Gene Expr. Patterns 5 (2004) 81–89.
[22] Y. Xi, G. Nakajima, J.C. Schmitz, E. Chu, J. Ju, Multi-level gene expression profiles affected by thymidylate synthase and 5-fluorouracil in colon cancer, BMC Genomics 7 (2006) 68.
[23] E.J. Gavin, B. Song, Y. Wang, Y. Xi, J. Ju, Reduction of Orc6 expression sensitizes human colon cancer cells to 5-fluorouracil and cisplatin, PLoS One 3 (2008) e4054.